

Environmental change on the eastern Arabian shelf during the early Aptian Oceanic Anoxic Event (OAE1a): A chemostratigraphic approach

Margherita Denaro^{*}, Thomas Steuber, Mohammad Alsuwaidi

Department of Earth Sciences, Khalifa University of Science and Technology, PO Box 127788, Abu Dhabi, United Arab Emirates

ARTICLE INFO

Editor: Bing Shen

Keywords:

Chemostratigraphy
Carbonate production
 $\delta^{13}\text{C}$ spatial distribution
Sediment preservation rate
Hawar Member
Shuaiba Formation

ABSTRACT

The effect of the early Aptian Oceanic Anoxic Event (OAE1a) on the southern Tethyan carbonate sedimentation on the eastern Arabian shelf is investigated. Chemostratigraphic platform-to-basin correlation of published and new outcrop and well core data allows for a lateral and temporal investigation of the changes in the depositional environment and reassessing the paleoenvironmental impact of OAE1a. Our results demonstrate that sedimentation rates varied spatially, influenced primarily by accommodation space and sediment redistribution rather than by effects of global carbon-cycle perturbations on carbonate production. Contrary to previous hypotheses, geochemical proxies do not support widespread anoxia on the Arabian shelf; instead, intermittent oxygen depletion was limited to specific basinal settings. Likewise, with the stratigraphic resolution of this study, no evidence of ocean acidification was detected, challenging models linking global carbonate platform demise to ocean acidification. Facies analysis reveals that transgressive-regressive cycles played a dominant role in shaping carbonate deposition. The transition from rudist–coral to orbitolinid–*Bacinella* assemblages reflects sea-level changes rather than nutrient stress. The spatial variations of $\delta^{13}\text{C}_{\text{carb}}$ indicate hydrodynamic isolation within the platform interior, affecting local carbon budgets. Sediment preservation rates align with other Tethyan carbonate platforms, reinforcing the role of sea-level fluctuations in controlling carbonate production and accumulation.

1. Introduction

The early Aptian perturbation of carbon-cycle dynamics, triggered by CO₂ emission associated with the emplacement of the Ontong-Java province, led to environmental changes that affected the carbonate factories of the Boreal and Tethys realms, which responded to the stressful conditions by reducing or ceasing carbonate production until the late Aptian–early Albian (Larson, 1991; Weissert et al., 1998; Wissler et al., 2003; Weissert and Erba, 2004; Tejada et al., 2009; Jenkyns, 2010; Skelton and Gili, 2012; Bottini et al., 2012; Erba et al., 2015; Bodin et al., 2015; Naafs et al., 2016; Amadio and Weissert, 2017; Adloff et al., 2020; Bauer et al., 2021; Percival et al., 2021). Greenhouse conditions and increasing weathering rates associated with changes in sea-water chemistry, including potential changes in pH, were suggested as possible causes of the dominance of mesotrophic assemblage, reduced genera diversification, extinction, and/or development of adaptative strategies as observed among rudist and calcareous nanoplankton (Erbacher et al., 1996; Masse et al., 1998; Wissler et al., 2003; Caldeira and Wickett, 2003; Erba and Tremolada, 2004; Erba et al., 2010, 2019;

Skelton and Gili, 2012; Steuber et al., 2023). Compared with the northern Tethys and central Atlantic, the evolution of carbonate production in the southern Tethys was significantly less affected (e.g. Erba et al., 1999; Pittet et al., 2002; Strohmenger et al., 2010; Skelton and Gili, 2012; Moullade et al., 2015; Amadio and Weissert, 2017; Castro et al., 2021; Steuber et al., 2022). In particular, the Arabian shelf represents an archive of carbonate sediments deposited during the OAE1a (Pittet et al., 2002; van Buchem et al., 2002; Immenhauser et al., 2005; Rameil et al., 2010; Strohmenger et al., 2010; Skelton and Gili, 2012; Yamamoto et al., 2013; Steuber et al., 2022; Jafarian et al., 2024; Alteneiji et al., 2024), which have been intensively studied as they host prolific hydrocarbon reservoirs. (e.g. Alsharhan, 1989; Sharland et al., 2001; Yose et al., 2006; van Buchem et al., 2010a, 2010b). The resilience of the Arabian Shelf stands in contrast to other regions of the Tethys where carbonate platforms experienced condensation or complete drowning during the same interval (Skelton and Gili, 2012). In this paper, a comprehensive chemostratigraphic platform-to-basin correlation of carbon-isotope records across the eastern Arabian shelf is presented. The identification of C-segments (Menegatti et al., 1998) and the

* Corresponding author.

E-mail address: KU100051936@alumni.ku.ac.ae (M. Denaro).

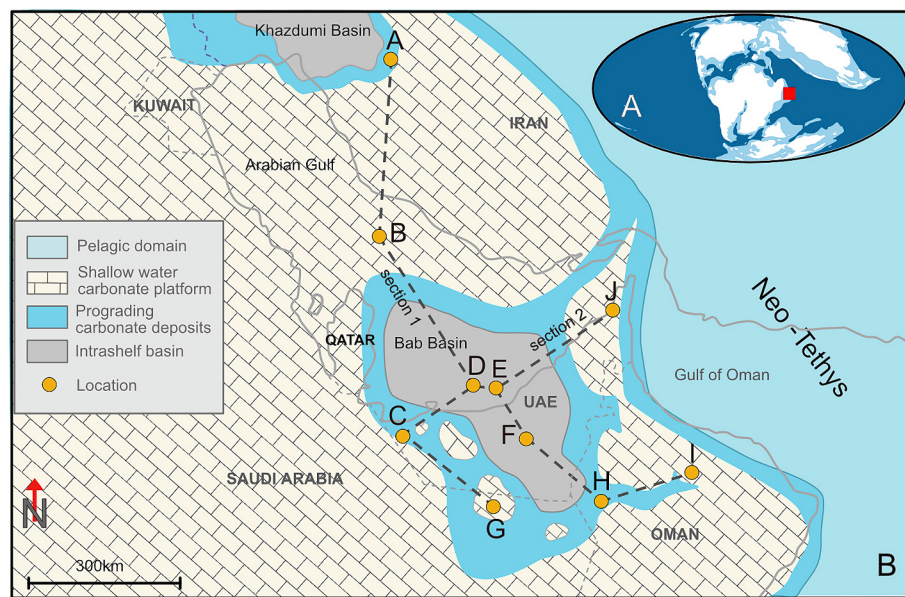


Fig. 1. A) Global palaeogeography, modified from Kocsis and Scotese (2021), red rectangle marks the study area. B) Late early Aptian palaeogeography of the Arabian Plate (modified from van Buchem et al., 2010a, 2010b; Alenejai et al., 2024). Sections 1 (N–S) and 2 (W–E) indicate the carbon-isotope curves correlation. Refer to Table 1 for details of localities. (For interpretation of the references to colour in this figure legend, the reader is referred to the web version of this article.)

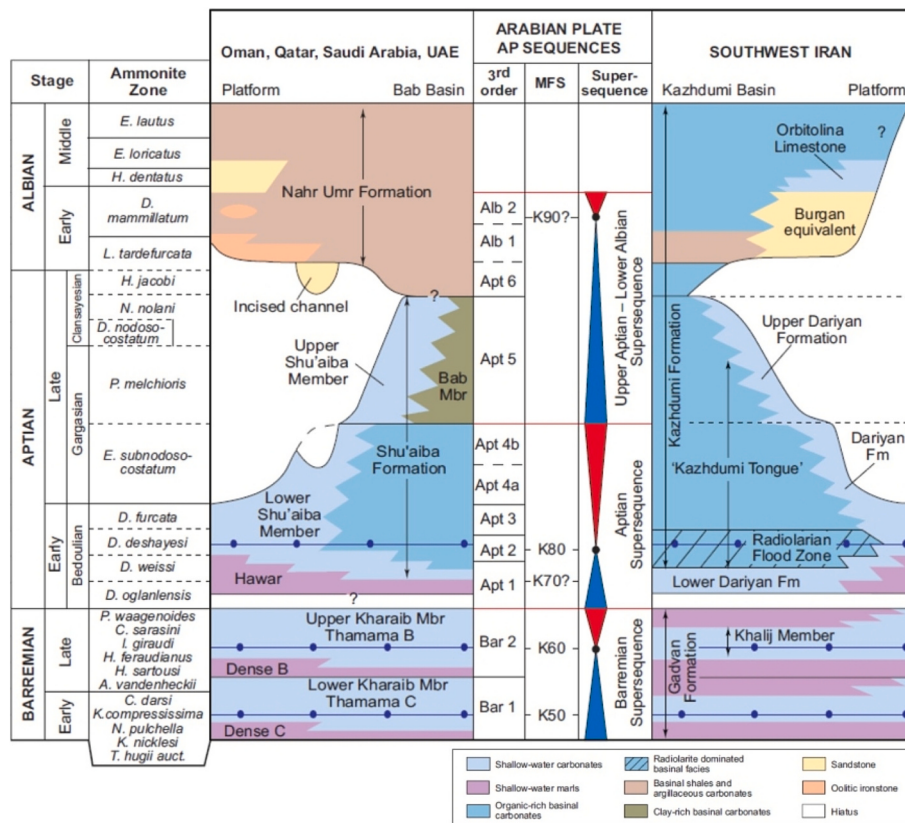


Fig. 2. Lithostratigraphy, sequence stratigraphy and biostratigraphy of the eastern Arabian plate (van Buchem et al., 2010b).

subdivision of the early Aptian carbon-isotope perturbation in “time slices” facilitated in-depth analysis of variations in carbon dioxide production and sedimentation rates around OAE1a, enabling a nuanced understanding of the interplay between global carbon-cycle disruptions and regional sedimentary dynamics. To validate the utility of chemostratigraphy and enhance its application in regional correlations, we

revisited the Wadi Mu’aydin (Oman) outcrop. High-resolution resampling of this outcrop was conducted to integrate chemostratigraphic data into an established stratigraphic framework based on biostratigraphy (Simmons and Hart, 1987; Schroeder et al., 2010), sequence stratigraphy, and sedimentological models (Sharland et al., 2001; Pittet et al., 2002; van Buchem et al., 2002, 2010a). The new data not only

replicate the carbon-isotope results reported by van Buchem et al. (2002) but also underscore the reproducibility and reliability of such measurements. This strengthens confidence in the chemostratigraphic methodology and reinforces its utility for correlating other stratigraphic sections within the study area, if the integrity of carbon isotope records and their diagenetic alteration is critically evaluated. Through this work, we aim to advance the understanding of sedimentation rate dynamics and carbon-isotope variability associated with OAE1a on the eastern Arabian shelf. This contributes to broader discussions on the environmental and geochemical impacts of early Aptian carbon-cycle perturbations.

2. Geologic setting

During the Lower Cretaceous, the Arabian Plate was located at equatorial latitude, c. 8° south (Hughes, 2000; Konert et al., 2001). The palaeogeography and passive-margin tectonic setting were favorable for the formation of an extensive carbonate depositional system (e.g. van Buchem et al., 2010a, 2010b; Droste, 2010) recorded in the Thamama Group (Habshan, Lekhwair, Kharaib and Shuaiba fms.), and the Wasia Group (Nahr Umr, Maaddud, Shilaif and Mishrif fms.). During the Barremian, the depositional system was a low-angle ramp ($<0.1^\circ$) that extended over thousands of kilometers (Fig. 1). Sedimentation was characterized by relatively pure carbonates throughout the ramp, with alternating periods of predominant siliciclastic sedimentation only in the northwest (van Buchem et al., 2010b; Pierson et al., 2010). The Barremian deposits of the Upper Lekhwair and Kharaib Formation in the UAE and Oman correspond to the time-equivalent Buwaib/Biyadh Formation in Saudi Arabia and the Gadvan Formation in Iran (Christian, 1997; Vincent et al., 2010; van Buchem et al., 2010b). The Dariyan Formation in Iran (Fig. 2) is time equivalent to the Shuaiba Formation (Christian, 1997; Vincent et al., 2010; van Buchem et al., 2010b). The coral/rudist-dominated sediments of the Kharaib Formation (or time equivalent sediments) are separated from the overlying orbitolinid-rich sediments of the Hawar Member by a regional unconformity that is also associated with the Barremian–Aptian boundary. In the early Aptian, the carbonate sedimentation over the shelf differentiated, resulting in the formation of two intrashelf basins: The Bab Basin, extending northwest-southeast for almost 600 km in the UAE and the Arabian Gulf, and the Kazhdumi Basin in the North (Sharland et al., 2001; Droste, 2010; Vincent et al., 2010; van Buchem et al., 2010b; Moosavizadeh et al., 2015). The intrashelf Bab Basin was surrounded by the shallow water carbonates of the Lower Shuaiba Mb. and became filled only during the late Aptian by the prograding Upper Shuaiba Fm. (Davies et al., 2002; Pierson et al., 2010; van Buchem et al., 2010a). The continued carbonate sedimentation was interrupted in the late Aptian–Albian by the deposition of the predominantly siliciclastic Nahr Umr Formation (van Buchem et al., 2002, 2010a; Simmons et al., 2007; Rameil et al., 2012; Strohmenger et al., 2010).

2.1. Regional stratigraphy

The Aptian carbon-cycle perturbations produced a characteristic carbon-isotope record, with a peak of the negative excursion typically hosted in the Hawar Mb., followed by a shift toward positive $\delta^{13}\text{C}$ values in the lower part of the Shuaiba Fm., which correlates with the Tethyan Livello Sellii (Coccioni et al., 1987). Numerous fluctuations of the carbon-isotope curve due to diagenetic overprint (e.g. Wadi Rahabaha, Alteneiji et al., 2024) may complicate the identification of the perturbation and its use for stratigraphic correlation. Therefore, chemostratigraphy must be calibrated to biostratigraphy and chronostratigraphy.

Orbitolinid biostratigraphic zonation of the Barremian–Aptian shallow-water carbonate systems of the eastern Arabian Plate is well-established (Schroeder, 1975; Simmons and Hart, 1987; Witt and Gökdag, 1994; Simmons, 1994; Simmons et al., 2000; Schroeder et al.,

2010) The presence of *Montseciella? arabica* in the Upper Kharaib Fm., as reported in Ras Al Khaimah, Jabal Akhdar and Jabal Madar (Pittet et al., 2002; van Buchem et al., 2002; Alteneiji et al., 2024) indicates a late Barremian–early Aptian age. The species *Palorbitolina ultima* and *Palorbitolina cormyi* found in the upper part of the Lower Shuaiba, indicate the late early Aptian. In Wadi Mu'aydin, the presence of *Mesorbitolina texana* in the Nahr Umr Fm. indicates the early–middle Albian (Simmons and Hart, 1987; Simmons, 1994).

Orbitolinid biostratigraphy is calibrated with calcareous nannofossil, planktonic foraminifer, and ammonite biostratigraphy, allowing for shallow-water to hemipelagic/pelagic correlation (Brälower et al., 1993; Erba et al., 1999; Mutterlose and Bottini, 2013; Granier, 2014; Moullade et al., 2015; Castro et al., 2021). The OAE1a, which extends over the isotopic segments C3–C6 (Menegatti et al., 1998) correlates with the *Globigerinelloides blowi* and *Leopoldina cabri* foraminifer zones (Lorenzen et al., 2013; Moullade et al., 2015; Castro et al., 2021). The event correlates also with the nannofossil zone NC6 and the *deshayesi* ammonite zone (Erba et al., 1999; Lorenzen et al., 2013; Moullade et al., 2015; Castro et al., 2021).

Based on Sr-isotope stratigraphy performed on unaltered shell material (Steuber et al., 2005), a late Barremian numerical age was derived for the upper part of the Kharaib Fm. (Strohmenger et al., 2010; Yamamoto et al., 2013) and a late early Aptian age for the top of the Lower Shuaiba (Strohmenger et al., 2010).

3. Materials and methods

Published carbon-isotope data from outcrops and well cores were utilized to correlate platform and basinal sections of the eastern Arabian shelf. This correlation was established using C-segment boundaries identified on the $\delta^{13}\text{C}$ curves as tie points. Given that each C-segment represents a specific time interval, this method allowed for a detailed assessment of variations in the carbonate environment and sedimentation rates throughout the OAE1a interval, shedding light on the relative contributions of elevated atmospheric CO₂ and relative sea-level fluctuations to the observed environmental changes.

The Wadi Mu'aydin outcrop is located in the Jebel Akhdar anticline, 15 km NE of Nizwa, Oman. Although the section was previously studied (Pittet et al., 2002; van Buchem et al., 2002; Al-Husseini and Matthews, 2010), the Upper Kharaib Fm. and Hawar Mb. were resampled at high resolution to verify the reproducibility and the robustness of carbon-isotope records related to different vertical sampling resolution and stable-isotope sampling strategies. From the 35.1 m outcrop section, 119 samples were collected with a constant sampling interval of 0.30 m. The section, starting at the road level (0 m), includes 11.5 m of the Upper Kharaib Fm. and the complete Hawar Mb.

The facies description is based on the petrographic analysis performed on thin sections using an Olympus BX51/52-P polarizing microscope with a digital camera Olympus DP72. The thin sections (thickness of 30 μm and polished) were impregnated with blue epoxy to highlight the porosity. The sample textures were classified based on the quantity of micrite/cement and the relation with skeletal/non-skeletal grains, their abundance, and size, following the textural classification of Dunham (1962) and Embry and Klovan (1971). Orbitolinid size was measured only on longitudinal sections of specimens presenting a well-preserved shape. The minimum number of measurements for each section was two specimens. The main components of the samples (orbitolinids, *Bacinella*, bioclasts, non-skeletal grains, micrite and interparticle cement) were estimated using the comparison charts from Bacchelli and Bosellini (1965).

XRF measurements of multi-element concentrations were performed using an Olympus InnovX Delta XRF Analyzer on washed and air-dried slabbed surfaces using 2-beam geochem mode with a beam time of 60 s each. Pure CaCO₃ (calcite), pure SiO₂ (quartz), NIST 2710a, and NIST 2711a were used to monitor instrument precision and reproducibility. The four standards were tested after every batch of ten samples to

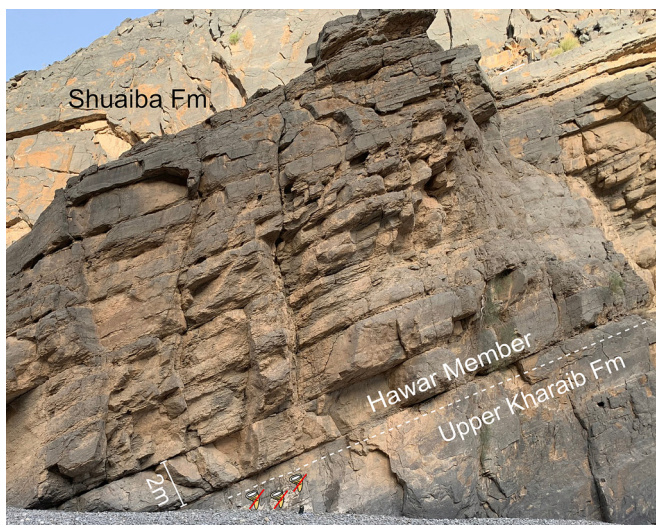


Fig. 3. Outcrop wall in Wadi Mu'aydin. The white dotted line indicates the erosive truncation of rudist bed. The Hawar Mb. is characterized by decimeter-scale beds.

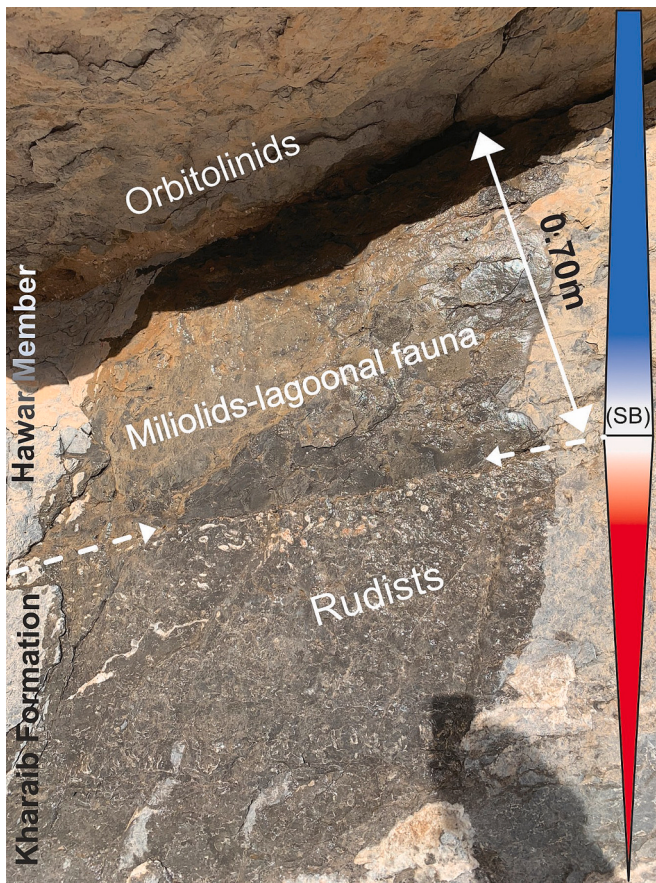


Fig. 4. Detail of the erosive truncation of rudist shells at the contact between Kharab Fm. and Hawar Mb.

monitor instrument drift. All the elements are reported in weight per cent (wt%) or parts per million (ppm). Based on the standards analysis, the precision of the results was better than 8 % of reported concentrations. Detection limits were 1000 ppm for Al, 50 ppm for S, 40 ppm for Mn and Fe, and 6 ppm for Sr.

Ca and Sr concentrations were considered indicative of carbonate

productivity fluctuations. Si, Ti, Zr, and Al, expressed as sum, were used as a siliciclastic proxy. Fe and Mn variations were used to investigate changes in paleo-redox conditions. Carbon and oxygen stable isotope analyses were performed on bulk carbonate samples. Two milligrams of powder were collected from each sample using a hand-held drill with tungsten drill bit of 0.6 mm diameter. Diagenetic cements were carefully avoided, and the sampling focused on micritic parts of the samples.

Isotopic measurements were performed by Elemtex Limited (UK) using a GasBench II linked to a DeltaPlus Advantage IRMS. Calibration was made using NBS18, NBS19, and Carrara marble standards. The results are reported in δ -values as the deviation in per mil from the Vienna Pee-Dee Belemnite (VPDB) standard. Reproducibility was generally better than 0.1 % for both $\delta^{13}\text{C}$ and $\delta^{18}\text{O}$ values.

The $\delta^{13}\text{C}$ contour maps were created using Surfer® software by applying to our dataset the natural neighbour algorithm (Yang et al., 2004). The method is based on an interpolation technique used when there are few missed data points in the dataset, creating a grid with continuous values within the dataset's maximum and minimum range. The maximum interpolation uncertainty is $\pm 0.45\ \text{\% } \delta^{13}\text{C}$.

4. Results and interpretations

4.1. Outcrop observations and facies identification

The studied outcrop section includes the upper part of the Kharab Fm. (one bed of 10.73 m thickness) and the overlying 23.6 m of the Hawar Mb. (Fig. 3). The Kharab bed is massive, with rudist clearly visible in the intervals 4.35–5.80 m and 8.70–10.73 m. The Kharab Fm.–Hawar Mb. boundary is marked by the erosive truncation of a rudist rudstone (Fig. 4). The Hawar Mb., in outcrop, can be easily differentiated from the Kharab Fm. by the presence of decimeter-scale beds of orbitolinid-rich limestone (van Buchem et al., 2002; Pittet et al., 2002). In the studied section, we have measured twenty-two decimeter-to-meter scale beds with bed thickness of 0.2 m–2.3 m. The Hawar Mb. represents the early transgressive phase of the 3rd order sequence (van Buchem et al., 2002). Burrows were observed in the upper part of the section in the interval between 27.2 and 28.5 m and between 32.7 and 34 m. Three depositional cycles were observed in the interval 31.5–35.10 m. Each cycle is marked by a shift in the visual appearance from brittle to more compact rock (Fig. 5). However, no major changes in facies or major elements composition were observed. The thinning upward trend of the sedimentary cycles is interpreted as a reduction of accommodation space (i.e. the space between seafloor and sea level). Based on the faunal content, texture and sedimentary structures, the facies (Table 2) agree closely with those described in the literature for the Kharab and Shuaiba Fm. (van Buchem et al., 2002, 2010a; Pittet et al., 2002; Strohmenger et al., 2006; Steuber et al., 2022; Alteneijer et al., 2024). Micrite is very abundant throughout the section, with dominant packstone and wackestone textures, indicating moderate to low-energy environmental conditions.

4.2. Elemental composition

The lithologies are pure carbonate with Ca concentrations of most samples between 36 and 40 % (Fig. 6). Only a few samples (at 5.7 m, 7.5 m, and 27.3 m) show Ca concentration of c. 32 %. Sr shows a slightly decreasing trend from bottom to top, with a higher concentration, around 400 ppm in the Kharab Fm. Similar values were reported in Bab Basin (Yamamoto et al., 2013) where, throughout the Kharab Fm. and Hawar Mb., Sr concentrations vary in the range of 300–500 ppm. Sr concentrations of bulk rock are difficult to interpret because of diagenetic alteration, specifically of originally Sr-rich aragonite, and uncertainties of the original mineralogical and elemental aragonite/calcite composition. Using Mn/Sr as a diagenetic proxy (Zhang et al., 2019; Stoll and Schrag, 2001; Steuber and Veizer, 2002; Brand and Veizer, 1980), there is a weak negative correlation, and Mn concentrations are



Fig. 5. Depositional cycles identified between 32 m and 35.10 m. M107 represents the position of the sample with an exceptionally low carbon-isotope value. M117 indicates the position of the last sample collected.

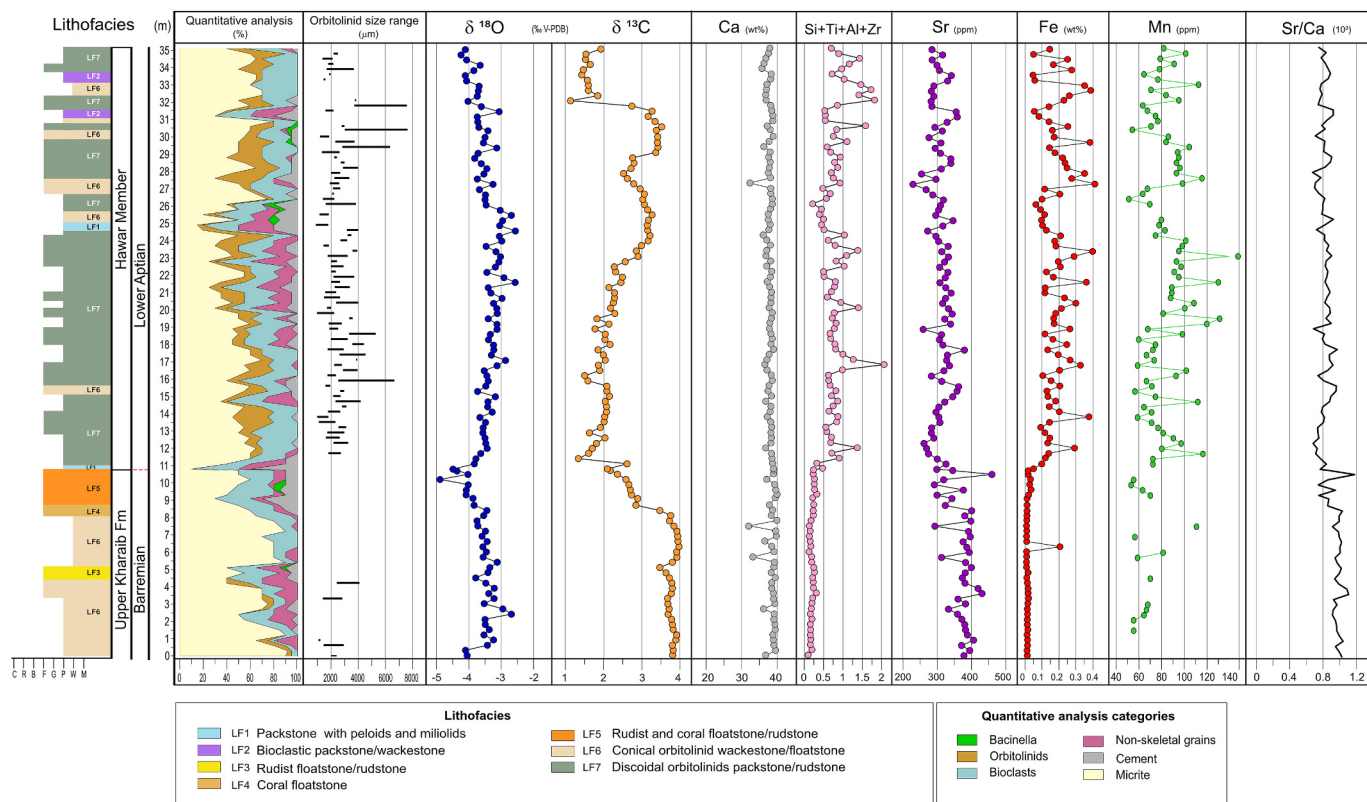


Fig. 6. Lithofacies, microfacies, and geochemistry of the upper Kharaiib Fm. and Hawar Mb. in Wadi Mu'aydin.

below the detection limit of 40 ppm in most samples of the Kharaiib Fm., where Sr concentrations are high (Figs. 6, 9C).

Based on the microscopic observations, the variations in Sr/Ca can be at least partially attributed to the original aragonite/calcite composition. The decreasing trend in the Sr/Ca ratio in the Wadi Mu'aydin section, starting from 8.5 m, is facies-dependent and coincides with the shifting from originally aragonite-rich rudist and coral-bearing sediments to orbitolinid facies. Fe concentrations are extremely low in the Kharaiib Fm (0–10.7 m), and on average 0.018 % while in the Hawar Mb., the concentrations vary in the range of 0.047–0.41 %. Siliciclastic

elements, expressed as the sum of Si, Ti, Zr and Al are very low and around 0.2 % in the Kharaiib Fm. In the Hawar Mb., the mean concentration is 0.8 %, with a maximum of 2.07 % at 16.8 m. Zr (4–17 ppm) is comparable with the concentrations observed in location J (Fig. 1). Those values suggest a limited terrigenous influence in the studied carbonate system when compared with the ~53 ppm of the Gulf of Mexico shallow-water carbonate platforms (Núñez-Useche et al., 2015) or with the ~135 ppm of the Aptian-Albian mixed siliciclastic-carbonate system of the Western African margin (Bonazzi et al., 2024).

The correlation of the siliciclastic trend of the studied section (Fig. 7)

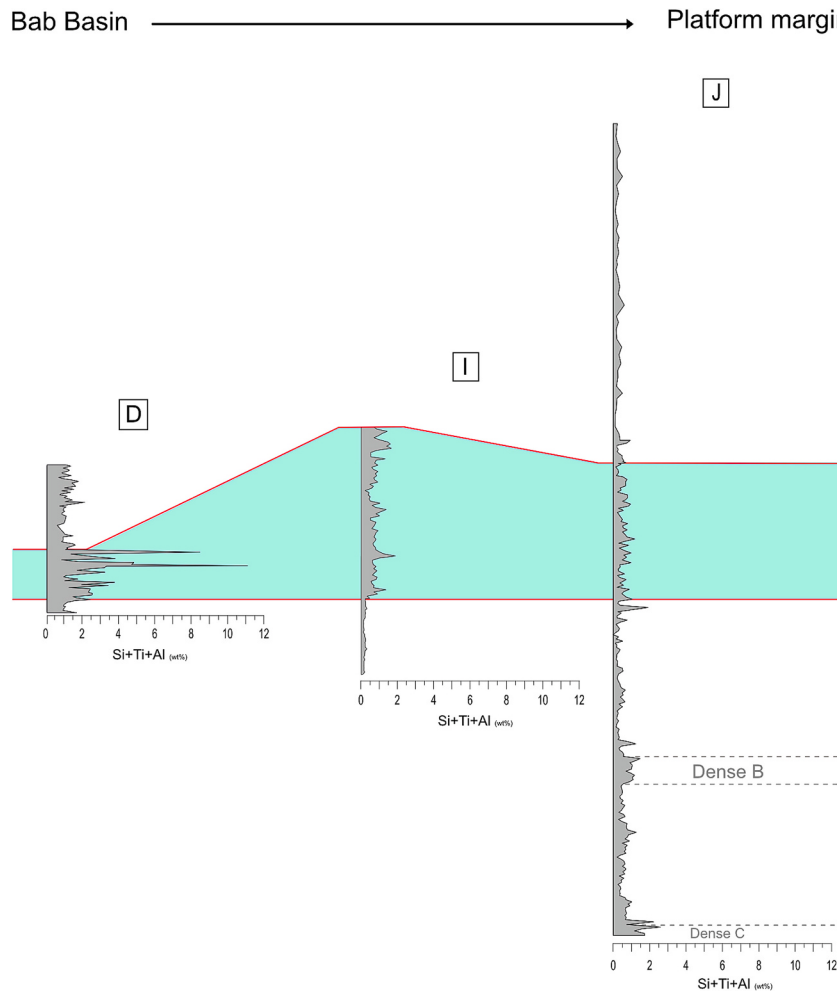


Fig. 7. Correlation of concentrations of siliciclastic elements of Wadi Mu'aydin (location I, this study), location J (Alteneiji et al., 2024), and location D (Steuber et al., 2022). Refer to Fig. 1 and Table 1 for locations. The Hawar Mb. is highlighted in green. (For interpretation of the references to colour in this figure legend, the reader is referred to the web version of this article.)

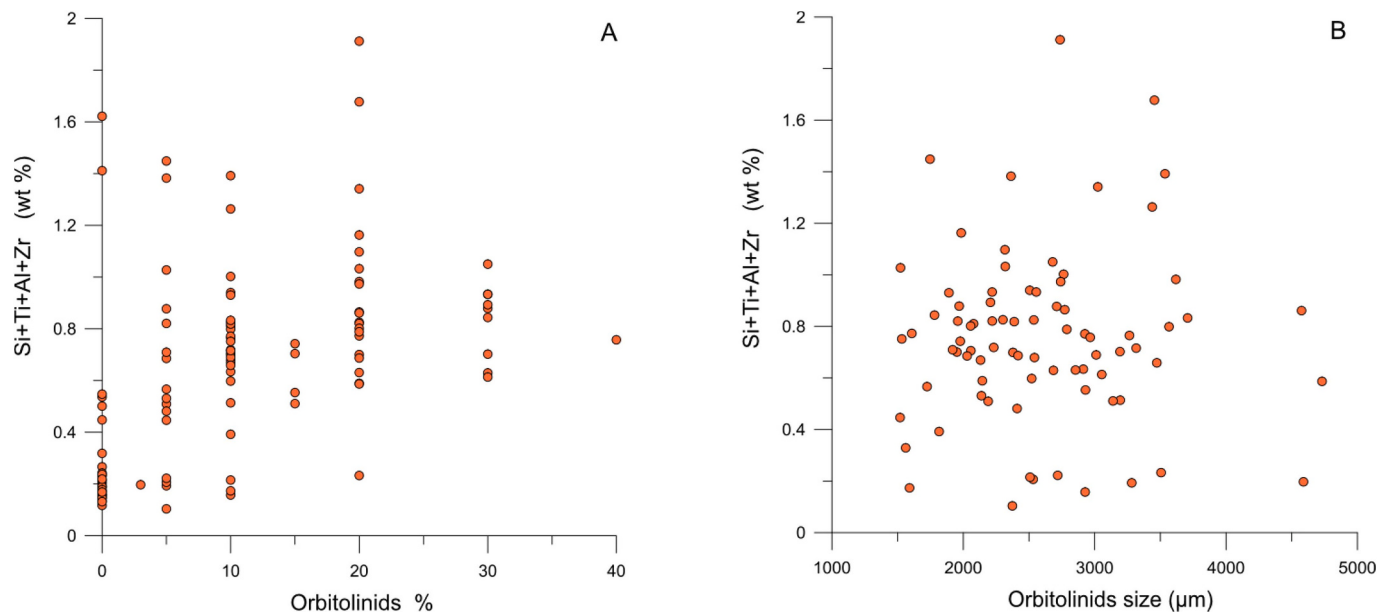


Fig. 8. A) Abundance of orbitolinids expressed as % of area in thin sections. B) Orbitolinids size versus siliciclastic content expressed as sum of elemental concentrations.

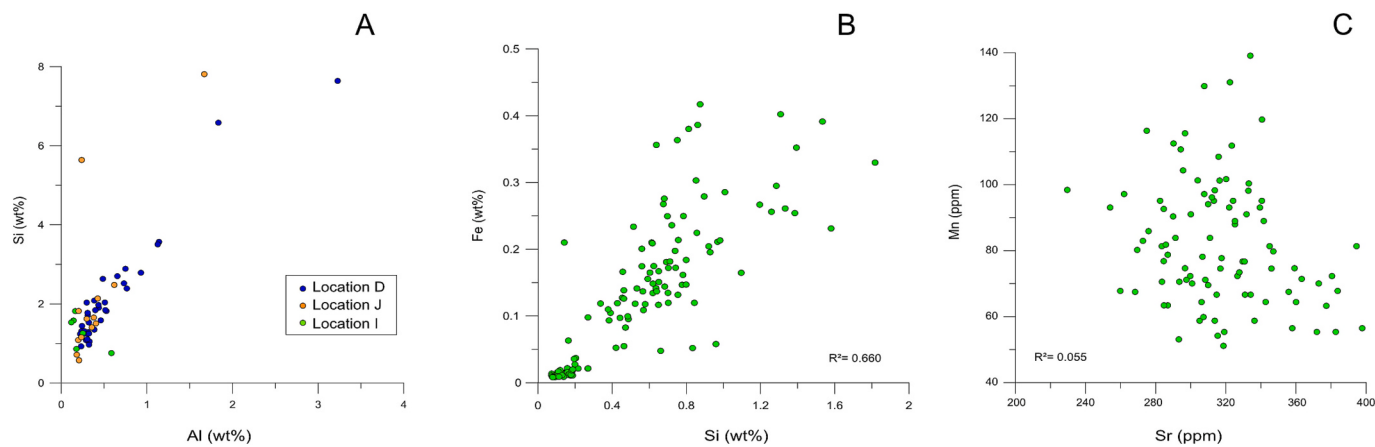


Fig. 9. Crossplots: A) Si vs. Al concentrations; B) Fe vs. Si concentrations; C) Mn vs Sr concentrations.

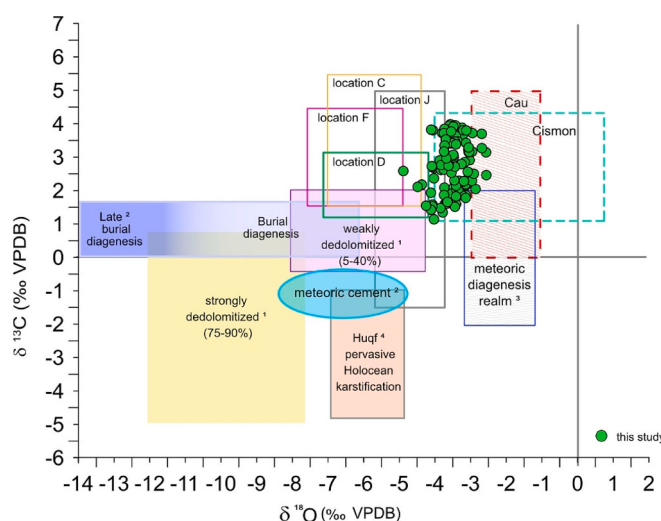


Fig. 10. Carbon and oxygen-isotope values of the studied locality (Wadi Mu'aydin, green dots) and values of localities of the eastern Arabian shelf (locations D (green rectangle), F (pink rectangle), C (yellow rectangle), J (grey rectangle) – refer to Fig. 1 and Table 1 for details), Cismon, Italy (Menegatti et al., 1998), Cau, Spain (Castro et al., 2021), and compared with ranges of values characteristic for diagenetic overprint; 1) Huck et al., 2017; 2) Immenhauser et al., 2003; 3) Immenhauser, 2021; 4) Sattler et al., 2005. (For interpretation of the references to colour in this figure legend, the reader is referred to the web version of this article.)

with location D and location J highlights that the site of the proto-Bab Basin was a preferential site of terrigenous material accumulation even if the Arabian shelf was considered to be a flat ramp when the Hawar Member was deposited (van Buchem et al., 2002). The riverine influx from the distant Al-Huqf High in the south and the Arabian Shield in the west followed a preferential route toward the Bab Basin or the Neo Tethys Ocean, excluding the eastern area (Pierson et al., 2010). The higher siliciclastics in the central part of the platform (location D) could have inhibited the carbonate deposition and triggered the initial differentiation between the basin and the platform. No correlation was found between the quantity of siliciclastics and the abundance of orbitolinids or their size (Fig. 8). The crossplot of Al versus Si (Fig. 9A) for locations D, J and I (this study) indicates that biogenic silica does not contribute significantly to the observed Si concentrations. Petrographic observations further support this interpretation, as no radiolaria or sponge spicules were identified in the thin sections.

The good correlation of Si and Fe concentrations (Fig. 9B), associated with S below the detection limit of 50 ppm in most samples and not

exceeding 1500 ppm in all samples studied, as well as the limited occurrence of pyrite in thin sections, suggest that Fe is predominantly associated with the detrital, siliciclastic fraction rather than authigenic mineral phases such as pyrite.

4.3. Stable carbon and oxygen isotopes

In the Wadi Mu'aydin section, the $\delta^{13}\text{C}_{\text{carb}}$ values vary from a maximum of 3.98 ‰ at 6.30 m to a minimum of 1.14 ‰ at 32.1 m (Fig. 6). Up to the top of the section at 35.1 m, the carbon-isotope values display only minor variations at around 1.5 ‰. The $\delta^{18}\text{O}_{\text{carb}}$ values vary in the range from -4.89 ‰ at 10.2 m to -2.56 ‰ at 21.6 m (Fig. 6). The oxygen-isotopic composition is typically altered during diagenesis so that the original signal cannot be expected to be preserved (e.g., Huck et al., 2017). Consequently, the oxygen-isotope record will not be further discussed. The low covariance between $\delta^{13}\text{C}_{\text{carb}}$ and $\delta^{18}\text{O}_{\text{carb}}$ values ($r^2 = 0.033$) indicates that diagenetic alterations had a limited impact on the carbon-isotope values (Fig. 10). This is also validated by comparing the data from this study with other published data from localities of the central and northern Tethys (Fig. 10). Despite the major tectonic events that involved the sedimentary succession of Wadi Mu'aydin (van Buchem et al., 2002), the samples present limited overprint of the carbon-isotope signal, similar to the range of values characteristic of the Cismon basinal sediments (Menegatti et al., 1998).

5. Discussion

5.1. C-segment identification of OAE1a

The $\delta^{13}\text{C}_{\text{carb}}$ data of Wadi Mu'aydin collected during this study were integrated with previous data from the same section (van Buchem et al., 2002; Al-Husseini and Matthews, 2010) and a composite curve was generated (Fig. 11). The curve was subdivided in C-segments following Menegatti et al. (1998), except for the C7/C8 boundary (Table 3). In this study, to facilitate an unequivocal recognition, the C7/C8 boundary was set at the maximum positive value of the $\delta^{13}\text{C}$ curve, following Herrle et al. (2004), and the C7 segment was named C7* to differentiate it from C7 as defined in Menegatti et al. (1998). Even though diagenetic alteration had a limited impact on the Wadi Mu'aydin carbon-isotope record, not all the C-segments could be identified. The C3 segment is characterized by a decreasing trend to the value of 1.14 ‰ $\delta^{13}\text{C}_{\text{carb}}$ in the Hawar Mb. The lower boundary of C3 was set at the value of 3.17 ‰ $\delta^{13}\text{C}_{\text{carb}}$ at around 81 m (Fig. 11). The lower boundary of C2 could not be placed confidently. C4 is characterized by a well-defined increasing trend from 1.32 ‰ to 4.56 ‰ $\delta^{13}\text{C}_{\text{carb}}$, interrupted by stable values around the level of 4.56 ‰, which define C5. The value of 0.6 ‰ in C5 was considered an outlier and not representative of the trend (Fig. 5). It

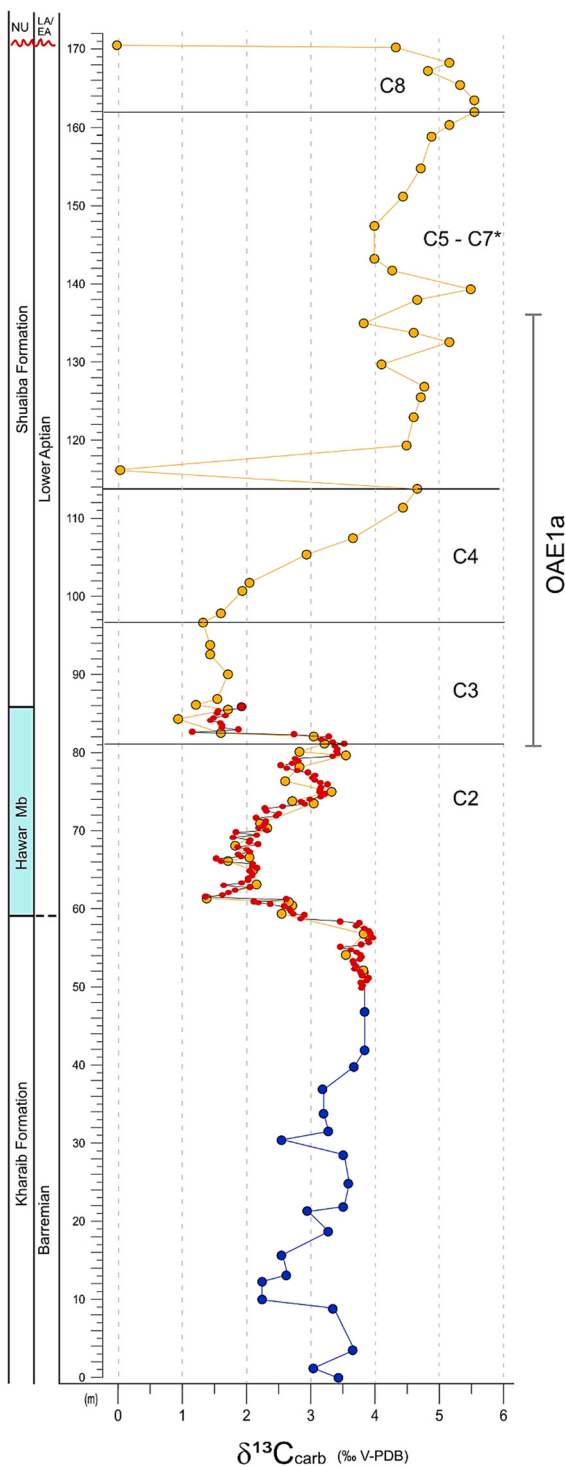


Fig. 11. Composite $\delta^{13}\text{C}_{\text{carb}}$ curve of the Wadi Mu'aydin section. Blue, $\delta^{13}\text{C}_{\text{carb}}$ curve from Al-Husseini and Matthews (2010); red, $\delta^{13}\text{C}_{\text{carb}}$ curve from this study. These results perfectly duplicate the carbon-isotope trend obtained by van Buchem et al. (2002) for the same outcrop (orange $\delta^{13}\text{C}_{\text{carb}}$ curve and data points), confirming the good reproducibility of the measurements. NU = Nahr Umr Fm. UA/A = upper Aptian/lower Albian. (For interpretation of the references to colour in this figure legend, the reader is referred to the web version of this article.)

was impossible to identify the upper boundary of C5, segment C6, and the lower boundary of C7*. Only the boundary C7*/C8 can be confidently placed at the inflection point to the decreasing value and set at 5.6 ‰ $\delta^{13}\text{C}_{\text{carb}}$.

Table 1
Localities of the eastern Arabian shelf used in the regional correlation.

LOCALITY	REFERENCES	SAMPLE TYPE
A Kuh-e-sefid, Iran	Moosavizadeh et al. (2013)	outcrop
B Well P, Arabian Gulf	Naderi-Khujin et al. (2016)	core
C1 Wells D, UAE	Strohmenger et al. (2010)	core
C2 Well E, UAE		core
D Well A, UAE	Steuber et al. (2022)	core
E Basinal section, UAE	Yamamoto et al. (2013)	core
F Asab field, well 322, UAE	Alsuwaidi (2015)	core
G Well H, Saudi Arabia	Al-Ghamdi and Pope (2014)	core
H Field Y, Oman	Vahrenkamp (2010)	core
I Wadi Mu'aydin, Oman	van Buchem et al. (2002); Al-Husseini and Matthews (2010).	outcrop
J Wadi Rahabah / Wadi Kebdah, UAE	This study. Alteneiji et al. (2024)	outcrop

5.2. Regional correlation

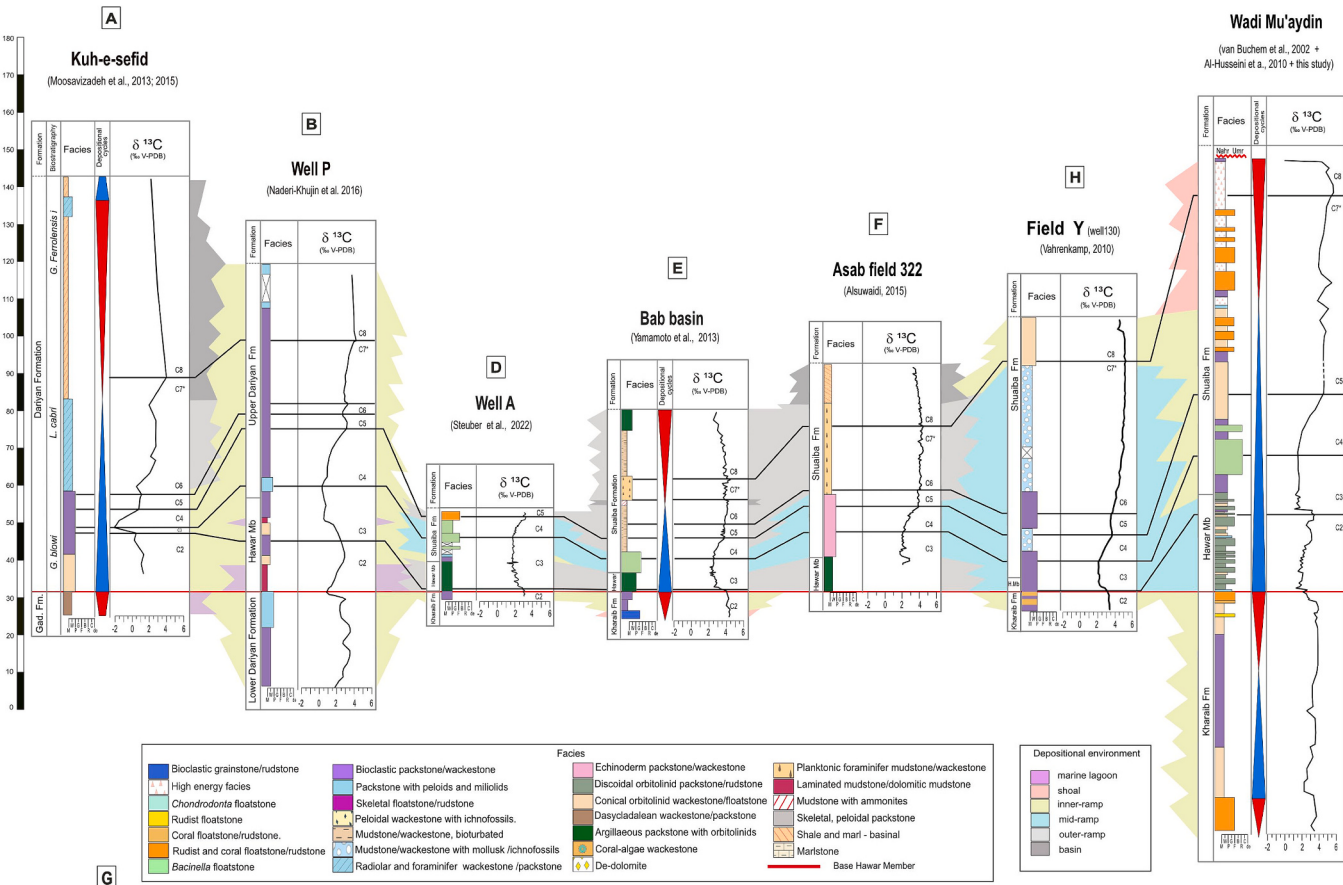
Each C-segment represents a time interval marked by changes in the carbon budget of the ocean, recorded in the sediment, and expressed by changes in the depositional environment and climate. The tie points identified in the Wadi Mu'aydin section were correlated with the same tie points identified in other published carbon-isotope curves available in the literature (Fig. 1, Table 1) for the UAE, Oman, Iran, and Saudi Arabia (van Buchem et al., 2002; Strohmenger et al., 2010; Vahrenkamp, 2010; Vincent et al., 2010; Al-Husseini and Matthews, 2010; Yamamoto et al., 2013; Moosavizadeh et al., 2013, 2015; Alsuwaidi, 2015; Al-Ghamdi and Pope, 2014; Naderi-Khujin et al., 2016; Steuber et al., 2022; Alteneiji et al., 2024). The curves were selected for correlation considering identifiable C-segments (Menegatti et al., 1998; Herrle et al., 2004). The regional correlation (N—S and W—E transects) is shown in Fig. 12.

5.3. Paleoenvironmental change related to OAE1a

5.3.1. Preset of the perturbation

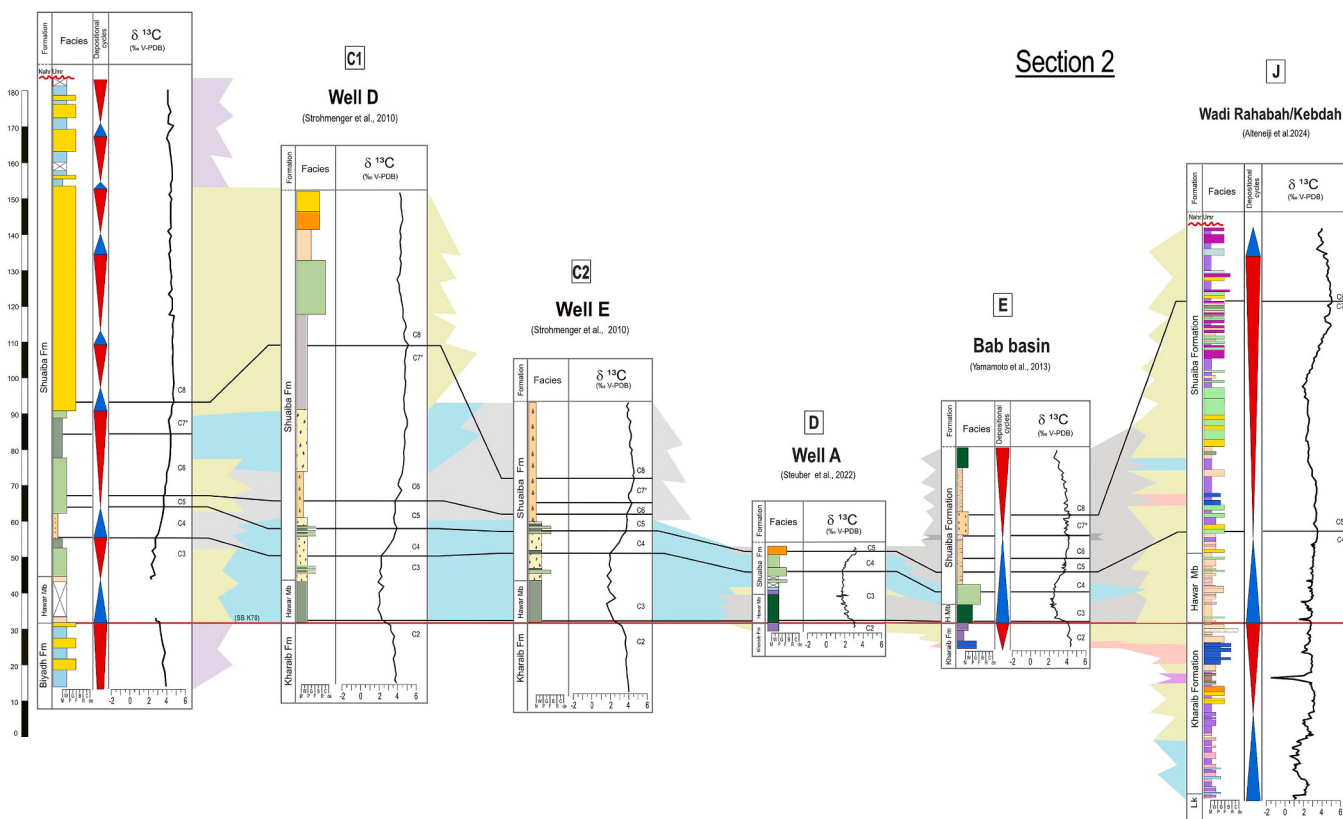
The C2/C3 boundary marks the onset of the ocean-atmosphere carbon cycle perturbation of OAE1a. Below this boundary, the sediments of the Upper Kharaiib, or its time equivalent Lower Darian and Biyadh formations, host the C2 segment which is late Barremian/early Aptian in age. The lack of carbon-isotope records or the effects of diagenesis makes it challenging to assign the lower C2 boundary to any of the carbon-isotope curves used for correlation. A regional subaerial exposure (SB K70) at the contact Kharaiib/Lower Darian/Biyadh Fm. with the Hawar Mb. (or time equivalent units) falls in the C2 segment and can serve as a helpful timeline. In Oman and the UAE, SB K70 is assigned to the sharp transition between granular sediment or rudist-bearing facies and the orbitolinid-dominated Hawar Mb. (van Buchem et al., 2002; Pittet et al., 2002; Hillgärtner et al., 2003; van Buchem et al., 2010a, 2010b; Granier and Busnardo, 2013). In Iran, this surface coincides with the contact between the argillaceous Gadvan Fm. and the Lower Darian Fm., while in Saudi Arabia, it falls at the top of the Biyadh Formation (Moosavizadeh et al., 2013, 2015; Al-Ghamdi and Pope, 2014). In Wadi Rahabah, at this level, no conclusive exposure features were observed, as de-dolomitization has obliterated any sign of the sedimentary structures (Alteneiji et al., 2024). In location E, no evidence of a hiatus was found, although, in Lekhwair-7, traces of rhizoliths testify to a paleosoil

Section 1



Well H

(Al Ghamdi and Pope, 2014)



(caption on next page)

Fig. 12. Regional correlation of the $\delta^{13}\text{C}_{\text{carb}}$ curves. The facies were unified by comparing the petrographic information provided in the references to the facies identified in this study. Facies different from those observed in Wadi Mu'aydin kept the original name. Section 1: N—S transect. Section 2: W—E transect; refer to Fig. 1 for locations. A) Kuh-e-sefid (Moosavizadeh et al., 2013). B) Well P (Naderi-Khujin et al., 2016). C1) Well D (Strohmenger et al., 2010). C2) Well E (Strohmenger et al., 2010). D) Well A (Steuber et al., 2022). E) Basinal section (Yamamoto et al., 2013). F) Asab field, well 322 (Alsuwaidi, 2015). G) Well H (Al-Ghamdi and Pope, 2014). H) Well Y (Vahrenkamp, 2010). I) Wadi Mu'aydin (van Buchem et al., 2002; Al-Husseini and Matthews, 2010; this study). J) Wadi Rahabah and Wadi Kebdah (Alteneiji et al., 2024; this study).

Table 2

Texture, description and depositional environments of the Wadi Mu'aydin section.

lithofacies	description	depositional environment
LF1: Packstone with peloids and miliolids	Dominated by miliolids and other small benthic foraminifers. Abundant peloids. Echinoderm fragments are identifiable, and on occasion, small shell fragments are present. Interparticle cement and micrite can be observed.	Restricted lagoon or middle ramp
LF2: Bioclastic wackestone/ packstone	Common bivalve shells, abundant echinoderm fragments, small foraminifera, miliolids, gastropods, occasional orbitolinids and rudist fragments. Bioclasts present margin corroded, partially to fully micritized. Occasionally recrystallized. Micrite is abundant. Rudist shells are abundant. The internal aragonitic layer of the rudist is recrystallized but still recognizable by the colour-contrast with the calcitic external layer and the dark micritic infill. In the micrite are also present abundant miliolids and echinoderm fragments. Occasional <i>Bacinella</i> is observed as an encruster on rudists and as lumps.	Inner to middle ramp
LF3: Rudist floatstone/ rudstone	Corals are associated with echinoderm fragments, small foraminifers and occasionally with conical orbitolinids. Rudist fragments were occasionally observed. Most of the corals are partially micritized. Interparticle space is filled with micrite, although locally recrystallized coral and sparite cement are continuous and the coral bioclasts are then barely identifiable. Occasionally, dasycladalean algae were observed.	Open lagoon or inner ramp
LF4: Coral floatstone	Rudists and corals are mostly well-preserved. Shell and echinoderm fragments are frequent. The matrix is mainly granular with abundant foraminifers and miliolids, locally peloidal.	Shoal or inner ramp
LF5: Rudist and coral floatstone/rudstone	Orbitolinids have conical test shapes. Occasionally partially micritized. Fragments of echinoderms, small foraminifers, and shell fragments are also present and abundant. Dasycladalean green algae are common. Few small <i>Bacinella</i> lumps are present.	Shoal or inner ramp
LF6: Conical orbitolinid wackestone/ floatstone	Orbitolinids appear discoidal and elongated, reaching a maximum diameter of 7 mm. The matrix varies from micritic to peloidal, with abundant echinoderm fragments. Rudist fragments, corals and <i>Bacinella</i> lumps have been observed occasionally.	Restricted lagoon, inner-middle ramp
LF7: Discoidal orbitolinid packstone/rudstone		Middle to outer ramp

development (van Buchem et al., 2002).

The topography of the eastern Arabian shelf at that time was a low-angle ramp that persisted until the boundary C3/C4. In localities C1, C2, D, E and H (Fig. 1, Table 1), the unconformity also coincides with the boundary C2/C3 (Fig. 12). On the contrary in localities A, B, and I (and potentially J), the SB/base of Hawar and the C2/C3 boundary do not coincide, showing a portion of the carbon-isotope record being absent in other localities. Seismic data excluded that during the C2 segment differential subsidence was active over the platform (Strohmenger et al., 2010) and comparison of siliciclastic influx between locations I and D (Fig. 7), would exclude that these locations developed conditions that slowed down or stopped the carbonate sedimentation at that time. It can be speculated that, after the late Barremian lowstand, the platform was gradually reflooded. Locations closer to the ocean margin (A, B, and I) were flooded first, recording part of the C2 signal in the sedimentary record, while the interior platform was exposed longer and flooded only later, leaving this part of the $\delta^{13}\text{C}_{\text{carb}}$ record unrecorded.

5.3.2. Negative CIE and Oceanic Anoxic Event 1a

The onset of the carbon-cycle perturbation is hosted in the C3 segment, marked by a negative carbon-isotope excursion (CIE) usually to $+1 - +2 \text{‰}$ $\delta^{13}\text{C}_{\text{carb}}$, except for locations A and B (Fig. 1, Table 1), which show lower values. The C3 segment covers part of the Hawar Mb. and Shuaiba Fm./upper Darian Fm. The Hawar Mb., in particular, is regarded as the expression of the carbon-cycle perturbation characterized by the replacement of coral and rudist with orbitolinid-rich facies, deposited during the early transgression of the 3rd order sequence Apt1 (van Buchem et al., 2010a). The change in trophic level was considered the reason for the proliferation of discoidal orbitolinids over the conical forms due to reduced light penetration (Pittet et al., 2002). Rudists, as filter feeders, thrive in water with elevated nutrient levels compared to corals, which although capable of inhabiting deeper settings, are generally more sensitive to turbidity. Nevertheless, both can occur in a mixed siliciclastic–calcareous depositional environment (Steuber et al., 2023). This observation challenges the actualistic assumption that Cretaceous corals were dominantly photosymbiotic and did not tolerate turbid water. The causal relation to explaining the disappearance of those biotas during C3 remains still elusive. In this context, the rise of the sea level could have played a critical role. Moreover, it should be considered that the transition rudist-orbitolinid-dominated facies is not an exclusive characteristic of the OAE1a but is also documented in the Barremian deposit of the Lekhwair and Kharaib fms. as expression of

Table 3

Synthesis table of the C-segments definition used in this study.

C1	Upper Barremian	$\delta^{13}\text{C}_{\text{carb}}$ values in the range of 2.0–2.8‰
C2		Decreasing trend toward 1.6–2.0 ‰ $\delta^{13}\text{C}_{\text{carb}}$
C3		Decreasing trend toward the minimum value of the $\delta^{13}\text{C}_{\text{carb}}$ curve (typically around 1.2–1.4 ‰)
C4		Abrupt increasing trend toward 4–5 ‰ $\delta^{13}\text{C}_{\text{carb}}$
C5	Lower Aptian	Decreasing or steady values with 0.2 ‰ $\delta^{13}\text{C}_{\text{carb}}$ amplitude
C6		Short increasing trend of around 1% $\delta^{13}\text{C}_{\text{carb}}$ amplitude
C7*		Short decreasing trend accompanied by an increasing trend toward the most positive value of the $\delta^{13}\text{C}_{\text{carb}}$ curve
C8		Values decreasing toward the pre-perturbation conditions (typically around 2‰ $\delta^{13}\text{C}_{\text{carb}}$)

Table 4

Duration of the C-segments (in Ma) calculated by different authors. In blue, duration and isotopic segments extension of the OAE1a. The bold numbers represent the minimum and maximum duration used for calculating the average duration of each C-segment: 358 kyr for C3, 274 kyr for C4, 540 kyr for C5 and 260 kyr for C6 (Beil et al., 2020; Charbonnier et al., 2023; Malinverno et al., 2010; Scott, 2016; Li et al., 2008; Martínez-Rodríguez et al., 2024).

LOCATION	METHODOLOGY	C1	C2	C3	C4	C5	C6	C7	C8	Duration OAE1a (Ma)
Vocontian Basin (Beil et al., 2020)	Cyclostratigraphy			0.433	0.388	0.281	0.315	1.345(?)	0.377(?)	1.42
Vocontian Basin (Charbonnier et al., 2023)	Cyclostratigraphy			0.485	0.262	0.296	0.247			1.29
Cismon APTICOR (Malinverno et al., 2010)	Orbital tuning			0.047	0.239	0.510	0.349	1.59		1.14
Cismon / Santa Rosa Canyon / Roter Sattel (Scott, 2016)	Graphic correlation using Cretaceous Chronostratigraphic Database CRETCSDB4	0.65	0.44	0.080	0.160	0.210	0.110	0.99	2 (?)	0.56
Cismon APTICOR (Li et al., 2008)	Cyclostratigraphy			0.041	0.33	0.570	0.330			1.27
La Bédoule (Moullade et al., 2015)	quantitative micropaleontology			0.289	0.318	0.289	0.260			1.15
Cau (Martínez-Rodríguez et al., 2024)	Cyclostratigraphy			0.230	0.230	0.870	0.140	0.470		1.47

Table 5

Thickness (m) of the C-segments for each locality used in the regional correlation (Fig. 12). Refer to Fig. 1 for locations. A) Kuh-e-sefid (Moosavizadeh et al., 2013). B) Well P (Naderi-Khujin et al., 2016). C1) well D (Strohmenger et al., 2010). C2) Well E (Strohmenger et al., 2010). D) Well A (Steuber et al., 2022). Bab Basin (Yamamoto et al., 2013). F) Asab field, well 322 (Alsuwaidi, 2015). G) Well H (Al-Ghamdi and Pope, 2014). H) Field Y (Vahrenkamp, 2010). I) Wadi Mu'aydin (van Buchem et al., 2002; this study).

LOCATION	C3	C4	C5	C6
A KUH-E-SEFID	2.3	4.61	3.84	
B WELL P	14.6	15	4.1	2.9
D WELL A	13	4.5		
E BAB BASIN	7.5	7.5	3.3	6.6
F ASAB FIELD		6.6	4.1	
C1 WELL D	19	8	7	
C2 WELL E	20	6	5	3
G WELL H		9	4	18
H FIELD Y	8.3	6.7	5.8	
I WADI MU'AYDIN	15	14.2		

transgressive/regressive cycles (Pittet et al., 2002).

The study of the siliciclastics trend (Fig. 7) has highlighted that location D received a major quantity of siliciclastics with respect to the distal areas of location I and J, and yet discoidal orbitolinid are present in location I. The lack of relationship between siliciclastics and orbitolinid size (Fig. 8) can be interpreted as supporting evidence that test size primarily reflects changes in water depth, rather than nutrient availability (Immenhauser et al., 1999; Simmons et al., 2000). Notably, the deposition of the Hawar Member during the OAE1a corresponds to a well-documented phase of relative sea-level rise on the Arabian Plate (Sharland et al., 2001; Haq, 2014). The higher quantity of siliciclastics in location D transported by an assumed riverine routing (Pierson et al., 2010), potentially triggered the differentiation between the basin and the shallow water domain. The decline in carbonate production in the central area contributed to the development of the Bab Basin, which was fully established by the end of the C4 segment and reached its maximum depth (60–100 m) during Apt3 (van Buchem et al., 2010b; Yose et al.,

2010). Meanwhile, the aggrading and then prograding marginal areas dominated by rudists and *Bacinella* accentuated the topographic contrast between the basin and its margins (Vahrenkamp, 1996; Yose et al., 2010). The smooth decreasing trend of the carbon-isotope curve in the C3 interval may be considered supporting evidence for a release of CO₂ over a long time interval (>10 kyr). This could validate the hypothesis of a pH fluctuation with stable carbonate saturation (Hönisch et al., 2012). In location D, Steuber et al. (2022) identified evidence of reduced carbonate saturation at the lowest value of the carbon-isotope curve, associated with the presence of a hardground and a subsequent reduction in Ca concentration to 20 %. In outcrop sections, detecting an acidification event is more challenging due to potential erosion or the absence of time-equivalent sediments, which may be only a few centimeters thick. Assuming the continuity of the isotopic record in the outcrop sections of Wadi Mu'aydin, the lowest value of the carbon isotope excursion (1.14 ‰ δ¹³C_{carb} at 32.1 m) does not co-occur with a remarkable decrease in calcium concentration and an increase in siliciclastics. In addition, biodiversity should be limited, dominated by species less affected by pH reduction such as orbitolinids (Steuber et al., 2022). Orbitolinids are found to be associated with algae, echinoderm fragments, peloids, miliolids (i.e., location B), and also rudist and other shell fragments (location H). The prolonged, constant and low δ¹³C_{carb} values observed in C3 after the peak negative excursion indicate a high sedimentation rate (Vahrenkamp, 2010). In location A, the sharp decreasing trend (−2 %) and the thin C3 segment compared with the regional trend (Fig. 12) suggest a low sediment preservation rate (condensation) due to the deepening of the area. By the combined effects of eustatic sea-level variations and tectonics, the Kazhdumi Basin started to develop already in the late Apt1 (Fig. 2), as suggested by the lateral change in facies, reaching its maximum depth of 125 m during Apt3 (van Buchem et al., 2010b; Vincent et al., 2010). Following the negative excursion, the trend of increasing δ¹³C_{carb} values due to the sequestration of isotopically light carbon in organic matter (C4–C6 interval) is biostratigraphically located in the middle-upper part of the *Globigerinelloides blowi* foraminifera zone (Menegatti et al., 1998). In location F, organic-rich sediments are described in C4 (Alsuwaidi, 2015), in the

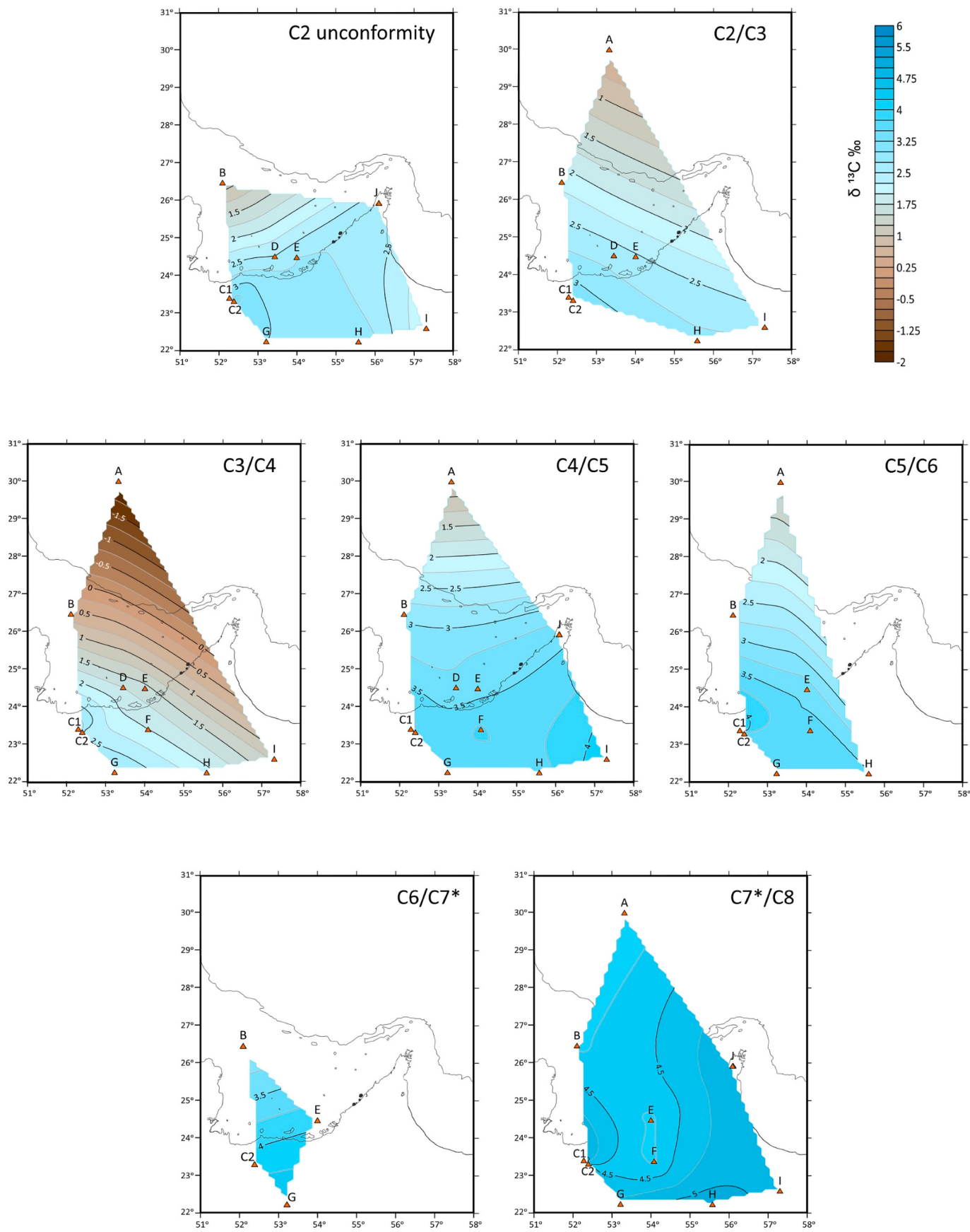


Fig. 13. Contour maps of $\delta^{13}\text{C}_{\text{carb}}$ variations from the preset to the recovery of OAE1a over the Eastern Arabian shelf. The number of data points varies for different C-segment boundaries, as not all could be identified in some sections (cf. Fig. 12).

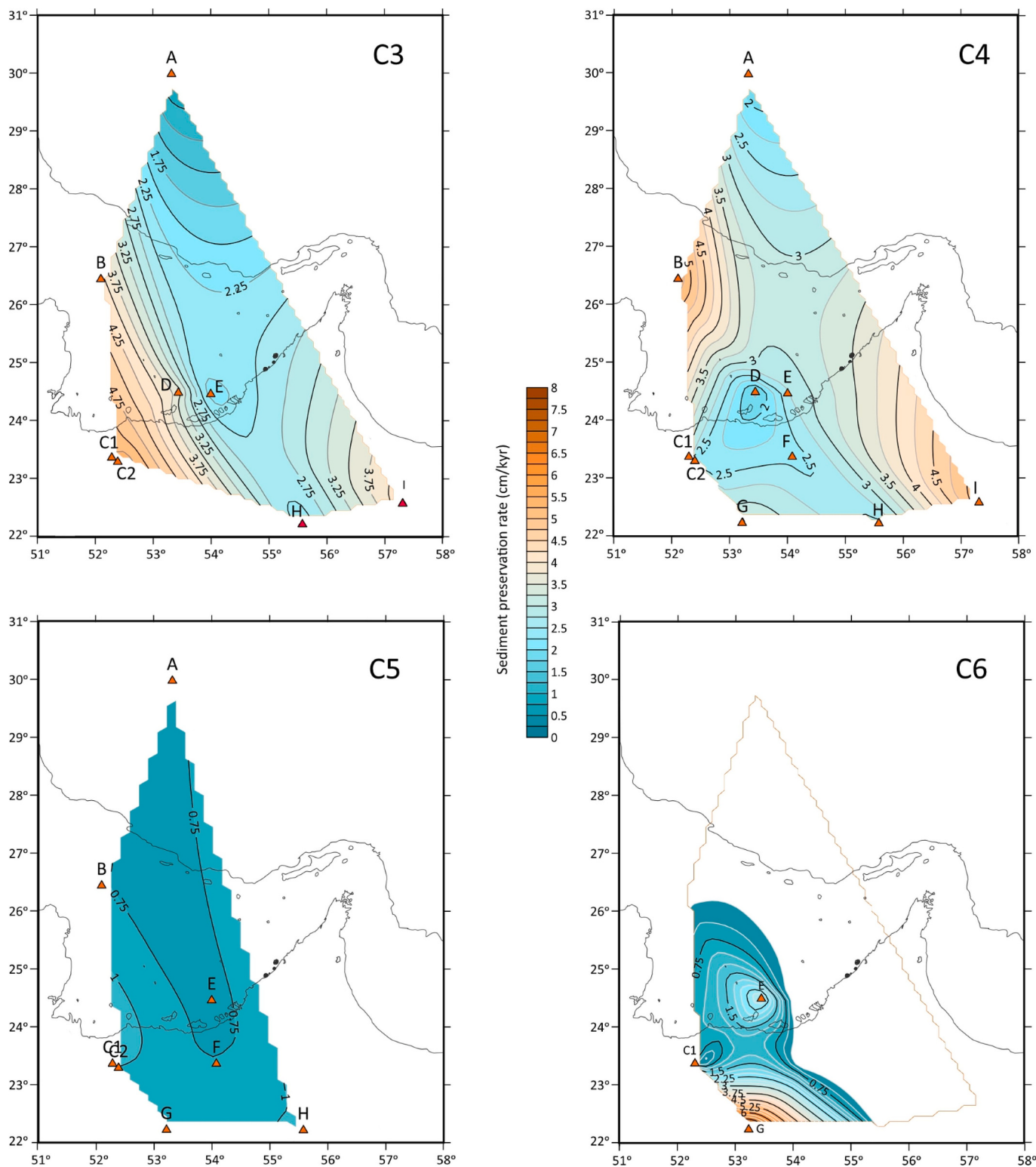


Fig. 14. Contour maps of sediment preservation rate during the C3–C6 intervals. The values are calculated considering the average duration of each segment between the maximum and the minimum values reported in Table 4 and the thickness of each C-segment at each location (Table 5).

mudstone/wackestone basinal facies with planktonic foraminifers that overlie the argillaceous sediments of C3. In location E organic-rich sediments appear only in C7 (Yamamoto et al., 2013). Black shales with high TOC of up to 18 %, as in the typical Selli Level (Baudin et al., 1998), are not encountered on the Arabian shelf. In the Bab and Kazhdumi basins, TOC reaches maximum values of 6 % (Alsuwaidi, 2015) and 3.5 % (Vincent et al., 2010; Jafarian et al., 2024), respectively. The

faunal assemblage of the C4–C6 interval is typical of oligo/mesotrophic conditions. *Bacinella*, which bloomed in the southern and central Tethys in this interval (Rameil et al., 2010; Immenhauser et al., 2005), benefitted from the ecological niche left by oligotrophic carbonate producers, affected by elevated nutrients. This microencruster is abundant in the Lower Shuaiba Fm. of locations C, G, I and J, while in the basin (locations D and E), it is limited to C4. In location J, *Bacinella*

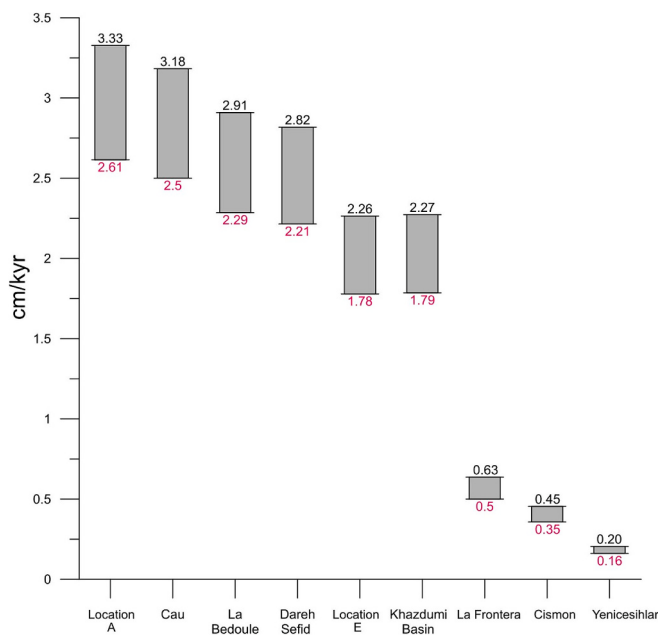


Fig. 15. Global comparison of OAE1a average sedimentation rates (C3-C6). The sedimentation rates were calculated for the duration of 1.1 Ma (black values) and 1.4 Ma (red values). Location A, Arabian Gulf (Naderi-Khujin et al., 2016); Cau, Spain (Castro et al., 2021); La Bédoule, France (Kuhnt et al., 2011); Darch Sefid, Iran (Jafarian et al., 2023); Location E -Bab Basin, UAE (Yamamoto et al., 2013); Khazdumi Basin, Iran (Jafarian et al., 2023); La Frontera - Subetic Basin, Spain (Herdicia and Maurrasse, 2025); Cismon- Belluno Basin, Italy (Menegatti et al., 1998); Yenicesihlar-Mudurnu Basin, Turkey (Hu et al., 2012). (For interpretation of the references to colour in this figure legend, the reader is referred to the web version of this article.)

structures proliferated in co-occurrence with low siliciclastics, suggesting a preference for a low-turbidity environment (Alteneiji et al., 2024). This ecological preference is consistently documented in the literature, and *Bacinella* is commonly found in limestones with a low argillaceous content (Rameil et al., 2010). This would explain the absence of *Bacinella* from the Bab Basin after the C4 interval, when the basin became too deep for phototrophic carbonate producers and received a significant amount of siliciclastics. A similar pattern is observed in the even deeper Khazdumi Basin (Fig. 1), where *Bacinella* is likewise absent in similar paleoenvironmental conditions (Jafarian et al., 2023). In contrast, *Bacinella* blooms on central Tethyan platforms are reported under markedly different conditions. In the Kanfanar section (Croatia), the proliferation coincides with a period of platform-top hypoxia, as indicated by redox-sensitive proxies, although it was concluded that *Bacinella* is not a universal indicator for hypoxic conditions (Hueter et al., 2019). In the Santa Maria and Monte Faito sections (central Italy), facies analysis and ecological interpretations suggest *Bacinella* thrived in mesotrophic to eutrophic conditions (Amodio and Weissert, 2017).

The presence of bioturbation in most of the sections of the eastern Arabian shelf, even the basinal ones (Fig. 12) argues for a well-oxygenated water column. The proximity with the Tethys Ocean, which would be the source of oxygenated water, would prevent the formation of anoxic water bodies on the platform, and for the upwelling of oxygen-depleted water from the Bab Basin to happen, anoxic conditions must exist in the basin. In location E, bioturbated sediments are reported during the C6 segment. The presence of organic matter and laminated sediments during C7 was considered by Yamamoto et al. (2013) to be indicative of anoxia due to high productivity and limited water circulation. However, no other supporting evidence, such as abundant pyrite, were reported. These observations suggest that anoxic conditions may have been rare and discontinuous over the Arabian shelf.

5.3.3. Recovery phase

On the eastern Arabian shelf, the return of the $\delta^{13}\text{C}_{\text{carb}}$ records to pre-perturbation values is a sign of recovery from the perturbation of OAE1a. In the Bab Basin, marly deposits with planktonic foraminifera and radiolarians continue to accumulate while, on the platform, facies dominated by corals and rudists re-appear. The only exception is for location A (Fig. 1, Table 1) where the outer ramp/basinal sedimentation continued. The reappearance of coral and rudist-dominated facies on the platform (localities G, C1, I, J) coincides with the early highstand of Apt3 (van Buchem et al., 2010a). A drier climate and limited weathering influx could have also contributed to re-establishing favorable ecological conditions. From C7* to C8 in the peri-basin area, the depositional environment becomes shallow (late HST-Apt4). A shoal environment is recorded in Wadi Mu'aydin with deposition of high-energy facies (van Buchem et al., 2002). In location J (Alteneiji et al., 2024) rudists dominate the top part with abundant *Agipoleura*, while lagoonal environments developed in location G. The Bab Basin began to be filled with the Upper Shuaiba sequences of the prograding basin margins (van Buchem et al., 2010a, 2010b).

5.4. Spatial variation of $\delta^{13}\text{C}$ values

The spatial variation in $\delta^{13}\text{C}_{\text{carb}}$ values across platform and basin locations at individual C-segment boundaries is illustrated with contour maps (Fig. 13). Notably, the southern interior platform regions exhibit consistently higher $\delta^{13}\text{C}_{\text{carb}}$ values compared to the northern, external platform throughout most of the intervals. This is opposite to the trend of increasing $\delta^{13}\text{C}_{\text{carb}}$ values from the platform to the basin which is expected due to reduced meteoric diagenesis, and enhanced organic matter accumulation in basinal areas (Immenhauser et al., 2002, 2003). On a smaller, regional scale, a platform-basin trend in $\delta^{13}\text{C}_{\text{carb}}$ values was also observed between the Bab Basin (locations D, E, and F) and its SW margin (locations C1 and C2) at all the C-segment boundaries. This trend was explained by the dominance of an aragonitic precursor along the platform margin, and the retention of higher $\delta^{13}\text{C}$ values of the aragonite during diagenetic stabilization to calcite (Swart and Eberli, 2005; Strohmenger et al., 2010). However, the large-scale pattern observed on the eastern Arabian shelf (Fig. 13) is not facies dependent. Consequently, the observed gradient must be related to large-scale processes operating on the vast carbonate platform of the eastern Arabian shelf. There is no modern analogue for such extensive carbonate depositional systems that were common on the flooded continental margins during Mesozoic episodes of high eustatic sea-level, with more than 600 km distance between the proximal and distal locations shown in Fig. 13. The balance between photosynthesis and respiration controls the vertical distribution of $\delta^{13}\text{C}$ of the dissolved inorganic carbon (DIC) in the open ocean, with photosynthesis dominating in the photic zone, and mineralization in the deeper water. This results in high $\delta^{13}\text{C}_{\text{DIC}}$ values in surface water when compared to the deep water of the ocean (e.g., Jahn et al., 2014; De Vincenzi Weirich et al., 2025). Exchange with the distant open ocean must have been limited for the interior parts of the eastern Arabian shelf so that a net preferential photosynthetic removal of ^{12}C will have resulted in high $\delta^{13}\text{C}_{\text{carb}}$ values in the interior platform. The contribution of DIC from continental sources with a low $\delta^{13}\text{C}$ by riverine drainage of the Arabian Shield must have been minimal.

During the recovery phase (C7*/C8), the isotopic values appear more uniformly distributed, regardless of the position on the shelf. This suggests a potential improvement of water circulation, possibly driven by changes in basin-platform mixing processes, reflecting the complex interplay between local hydrodynamics, sedimentary processes, and platform morphology.

5.5. Sediment preservation rates

The duration of the OAE1a (C3-C6) appears to be relatively well constraint from several studies and using different methods, ranging

between 1.1 and 1.4 My (Table 4). However, significant discrepancies exist in the estimated duration of individual C-segments due to variations in the preservation of the sedimentary record, possible hiatuses, condensation, or different approaches to the division of C-segments, and the time scales used. Here, the sediment preservation rates across the eastern Arabian shelf were calculated by dividing the thickness of each C-segment (Table 5) by the average reported duration of the corresponding C-segment (Table 4). This approach assumes continuity in the sedimentation record and simplifies the analysis by avoiding widely varying maximum and minimum duration estimates, which may be biased by incomplete or inconsistent data. The mean durations considered for the analyses are 358 kyr for C3, 274 kyr for C4, 540 kyr for C5 and 260 kyr for C6.

Duration of the C-segments shorter than 100 kyr produced unrealistic high rates and are excluded. Contour maps of sediment preservation rates were created to illustrate the distribution over the eastern Arabian shelf (Fig. 14). The OAE1a is associated with two-3rd-order transgressive-regressive cycles (van Buchem et al., 2002). During C3, which represents the early phase of the transgression, the platform localities (B, C1, C2, I) present a sediment preservation rate between 4 and 5.59 cm/kyr. Over C4, high sedimentation rates are evident close to the former platform margin. No data are available for C5 and C6 for this area. The location of the proto-Bab Basin is characterized by values between 2 and 3.63 cm/kyr, with the exclusion of locality A, which has the lowest value (0.70 cm/kyr) during C3. This low sediment preservation rate in the Fars area could indicate that during C3, the carbonate production was reduced compared to more southern localities. It is interesting to observe a substantial difference in sedimentation rate between localities D, E and I, although during the interval C3, argillaceous orbitolinid-rich facies were deposited in these localities. At the end of C3, the creation of accommodation space was facilitated by rapid sea level rise, as suggested also by constant $\delta^{13}\text{C}_{\text{carb}}$ values around +1 – +2 ‰ preceding the positive trend of C4. With the highstand (C5), subsidence was the only contributor to the creation of accommodation space on the platform. The sediments produced were forced to prograde into the newly formed intrashelf basins, where the accommodation space outpaced the sediment production (condensation). The redistribution of carbonate sediment is reflected in a uniformly low preservation rate (average 0.86 cm/kyr) during the C5 segment (Fig. 14).

Considering the total duration of OAE1a (1.1–1.4 Ma), the sediment preservation rate for the platform section Well P is calculated to be 2.61–3.33 cm/kyr, based on a 36.6 m thick C3–C6 interval. These values (Fig. 15) are similar to those obtained for platform margin and hemipelagic localities such as La Bédoule (Kuhnt et al., 2011), Cau (Castro et al., 2021), and Dareh Sefid (Jafarian et al., 2023). At location E, where the C3–C6 interval measures 24.9 m in thickness, the calculated sediment preservation rate aligns closely with the Kazhdumi Basin (Jafarian et al., 2023). However, it is three to five times higher than in the Belluno Basin (Menegatti et al., 1998), and the Subbetic Basin (Herdicia and Maurrasse, 2025), and even 10 times higher than the Mudurnu Basin (Hu et al., 2012). The sediment preservation rates estimated for both locations B and E are consistent with previously reported Cretaceous sediment preservation rates of 2.16 cm/kyr for the Shuaiba Formation and 3.6 cm/kyr for the Arabian Gulf (Bosscher and Schlager, 1993). Furthermore, they fall within the range of Cretaceous accumulation rates calculated for other carbonate systems such as the Bahamas platform and the Atlantic margin (2.6–8 cm/kyr, Bosscher and Schlager, 1993). When the sediment preservation rate estimated for the eastern Arabian shelf during OAE1a is compared with preservation rates documented for carbonate platforms throughout Earth's history (e.g., Bosscher and Schlager, 1993), it becomes clear that the observed values do not reflect a reduction in carbonate production. This interpretation is reinforced by the accepted recognition that sediment preservation rates are typically one to several orders of magnitude lower than production rates, and decrease with the duration of the stratigraphic interval considered (Schlager, 2003; Pohl et al., 2020). The recognition of

clinoforms in the Bab Basin reflects the transfer of sediment from the Upper Shuaiba platform into the basin (Maurer et al., 2010), supporting the observation that the OAE1a did not significantly impair the carbonate production of the region studied. Instead, relative sea-level fluctuations likely played a major role influencing the carbonate accumulation and preservation.

6. Conclusions

By correlating platform-to-basin sections over the eastern Arabian shelf using identifiable C-segments we were able to reconstruct spatial and temporal variations in depositional settings and identify key processes that governed carbonate production and preservation during the OAE1a. Novel insights into early Aptian carbonate platform dynamics were presented by quantifying spatial variations in both $\delta^{13}\text{C}_{\text{carb}}$ signatures and sediment preservation rates across the region. A pronounced gradient in $\delta^{13}\text{C}_{\text{carb}}$ values is documented, with the southern, interior parts of the platform characterized by $\delta^{13}\text{C}_{\text{carb}}$ values compared to the northern and external platform and basinal settings. This pattern reflects the effects of hydrodynamic isolation within the platform interior and the sustained photosynthetic sequestration of ^{12}C within the photic zone.

The estimation of sediment preservation rates across the C3–C6 interval reveals the limited response of the carbonate factory to the OAE1a perturbation. Sediment preservation rates of Arabian platform locations are consistent with values from other early Aptian Tethyan carbonate systems and Phanerozoic sediment preservation rates in general. Geochemical proxy data do not support the occurrence of widespread anoxia across the Arabian shelf. Oxygen-depleted conditions appear to have been spatially restricted and temporally intermittent, confined to specific basinal environments without consistent development of an anoxic water column. Similarly, there is no sedimentological or geochemical evidence for ocean acidification affecting shallow-water carbonate factories.

The results of this study suggest that sea-level fluctuations and regional hydrodynamics strongly modulated the regional environmental and sedimentary response, different from platform demise during OAE1a in higher latitudes.

CRediT authorship contribution statement

Margherita Denaro: Writing – review & editing, Writing – original draft, Visualization, Investigation, Formal analysis, Data curation.

Thomas Steuber: Writing – review & editing, Writing – original draft, Visualization, Validation, Supervision, Project administration, Investigation, Funding acquisition, Data curation.

Mohammad Alsuwaidi: Writing – review & editing, Project administration, Investigation, Funding acquisition.

Declaration of competing interest

The authors declare that they have no known competing financial interests or personal relationships that could have appeared to influence the work reported in this paper.

Acknowledgements

This work was supported by Khalifa University of Science and Technology grant CIRA 2019-203. D. Hennhoefer and F. Schlagintweit are thanked for their help and suggestions during the field campaign and the initial stage of the project. The constructive comments of two reviewers helped to improve the original submission and are gratefully acknowledged.

Appendix A. Supplementary data

Supplementary data to this article can be found online at <https://doi.org/10.1016/j.palaeo.2025.113225>.

Data availability

The authors confirm that all data necessary for supporting the scientific findings of this paper have been provided.

References

- Adloff, M., Greene, S.E., Parkinson, I.J., Naafs, B.D.A., Preston, W., Ridgwell, A., Lunt, D.J., Castro Jiménez, J.M., Monteiro, F.M., 2020. Unravelling the sources of carbon emissions at the onset of Oceanic Anoxic Event (OAE) 1a. *Earth Planet. Sci. Lett.* 530, 115947. <https://doi.org/10.1016/j.epsl.2019.115947>.
- Al-Ghamdi, N., Pope, M., 2014. Integrated high-resolution chemostratigraphy and facies-based stratigraphic architecture of the lower Cretaceous (Aptian), Shu'aiba Formation, Saudi Arabia. *Am. Assoc. Pet. Geol. Bull.* 98 (8), 1521–1549. <https://doi.org/10.1306/05161311194>.
- Al-Husseini, M.I., Matthews, R.K., 2010. Tuning late Barremian–Aptian Arabian Plate and global sequences with orbital periods. In: van Buchem, F.S.P., Al-Husseini, M.I., Maurer, F., Droste, H.J. (Eds.), Barremian–Aptian Stratigraphy and Hydrocarbon Habitat of the Eastern Arabian Plate, vol. I. *GeoArabia Special Publication 4*, pp. 199–228.
- Alsharhan, A.S., 1989. Petroleum geology of the United Arab Emirates. *J. Pet. Geol.* 12 (3), 253–288. <https://doi.org/10.1111/j.1747-5457.1989.tb00197.x>.
- Alsuwaidi, M.E., 2015. Lower Bab Member (AO): A Study of Sequence Stratigraphy, Porosity Characterization and Tight Reservoir Development. Colorado School of Mines, Abu Dhabi, UAE. Ph.D. Thesis.
- Altenejji, N., Denaro, M., Schlagintweit, F., Alsuwaidi, M., Hennhoefer, D., Steuber, T., 2024. The Barremian–lower Aptian of NE Arabia: the Kharaib and Shu'aiba formations in Wadi Rahabah and Wadi Kebdah, Ras Al Khaimah U.A.E. *Cretac. Res.* 159, 105873. <https://doi.org/10.1016/j.cretres.2024.105873>.
- Amodio, S., Weissert, H., 2017. Palaeoenvironment and palaeoecology before and at the onset of Oceanic Anoxic Event (OAE) 1a: reconstructions from Central Tethyan archives. *Palaeogeogr. Palaeoclimatol. Palaeoecol.* 479, 71–89. <https://doi.org/10.1016/j.palaeo.2017.04.018>.
- Baccelle, L., Bosellini, A., 1965. Charts for visual estimation of the percentage composition in sedimentary rocks. *Geol. Soc. Paleontol.* 1, 59–62.
- Baudin, F., Fiet, N., Coccioni, R., Galeotti, S., 1998. Organic matter characterisation of the Sellì Level (Umbria-Marche Basin, Central Italy). *Cretac. Res.* 19 (6), 701–714. <https://doi.org/10.1006/cres.1998.0126>.
- Bauer, K.W., Bottini, C., Frei, R., Asael, D., Planavsky, N.J., Francois, R., McKenzie, N.R., Erba, E., Crowe, S.A., 2021. Pulsed volcanism and rapid oceanic deoxygenation during Oceanic Anoxic Event 1a. *Geology* 49 (12), 1452–1456.
- Beil, S., Kuhnt, W., Holbourn, A., Scholz, F., Oxmann, J., Wallmann, K., Lorenzen, J., Aquit, M., Chellai, E.H., 2020. Cretaceous oceanic anoxic events prolonged by phosphorus cycle feedbacks. *Clim. Past* 16 (2), 757–782. <https://doi.org/10.5194/cp-16-757-2020>.
- Bodin, S., Meissner, P., Janssen, N.M., Steuber, T., Mutterlose, J., 2015. Large igneous provinces and organic carbon burial: Controls on global temperature and continental weathering during the early Cretaceous. *Glob. Planet. Chang.* 133, 238–253. <https://doi.org/10.1016/j.gloplacha.2015.09.001>.
- Bonazzi, M., Bonacina, G., Massara, E.P., Piva, A., Scotti, P., Viaggi, P., Sanfilippo, A., 2024. Reconstructing redox variations in a young, expanding ocean basin (Cretaceous Central Atlantic). *Cretac. Res.* 153, 105681. <https://doi.org/10.1016/j.cretres.2023.105681>.
- Bosscher, H., Schlager, W., 1993. Accumulation rates of carbonate platforms. *J. Geol.* 101 (3), 345–355. <https://www.jstor.org/stable/30065789>.
- Bottini, C., Cohen, A.S., Erba, E., Jenkyns, H.C., Coe, A.L., 2012. Osmium-isotope evidence for volcanism, weathering, and ocean mixing during the early Aptian OAE 1a. *Geology* 40 (7), 583–586. <https://doi.org/10.1130/g33140.1>.
- Bralower, T.J., Sliter, W.V., Arthur, M.A., Leckie, R.M., Allard, D., Schlanger, S.O., 1993. Dysoxic/anoxic episodes in the Aptian-Albian (early Cretaceous). *Geophys. Monogr. Ser.* 77, 5–37.
- Brand, U., Veizer, J., 1980. Chemical diagenesis of a multicomponent carbonate system; I. Trace elements. *J. Sediment. Res.* 50 (4), 1219–1236.
- Caldeira, K., Wickett, M.E., 2003. Anthropogenic carbon and ocean pH. *Nature* 425, 365. <https://doi.org/10.1038/425365a>.
- Castro, J.M., Ruiz-Ortiz, P.A., de Gea, G.A., Aguado, R., Jarvis, I., Weissert, H., Molina, J.M., Nieto, L.M., Pancost, R.D., Quijano, M.L., et al., 2021. High-resolution C-isotope, TOC and biostratigraphic records of OAE 1a (Aptian) from an expanded hemipelagic cored succession, western Tethys: A new stratigraphic reference for global correlation and paleoenvironmental reconstruction. *Paleoceanogr. Paleoclimatol.* 36 (3). <https://doi.org/10.1029/2020pa004004>.
- Charbonnier, G., Boulila, S., Spangenberg, J.E., Vermeulen, J., Galbrun, B., 2023. Astrochronology of the Aptian stage and evidence for the chaotic orbital motion of Mercury. *Earth Planet. Sci. Lett.* 610, 1118104. <https://doi.org/10.1016/j.epsl.2023.1118104>.
- Christian, L., 1997. Cretaceous subsurface geology of the Middle East Region. *GeoArabia* 2 (3), 239–256.
- Coccioni, A., Nesci, O., Tramontana, M., Wezel, F.C., Moretti, E., 1987. Descrizione di un livello-guida "Radiolarito-bituminoso ittiolitico" alla base delle marne a fucoidi nell'Appennino umbro-marchigiano. *Boll. Della Soc. Geol. Ital.* 106 (1), 183–192.
- Davies, R.B., Casey, D.M., Horbury, A.D., Sharland, P.R., Simmons, M.D., 2002. Early to mid-Cretaceous mixed carbonate-clastic shelfal systems: examples, issues and models from the Arabian Plate. *GeoArabia* 7 (3), 541–598. <https://doi.org/10.2113/geoarabia0703541>.
- De Vincenzi Weirich, Y.S., da Costa Machado, E., Carlos, L.C., Rocha, E.B., Muniz, M.C., dos Anjos, R.M., Mendes, C.R.B., Kerr, R., 2025. Controls on the spatial variability of $\delta^{13}\text{C}_{\text{DIC}}$ along the Bransfield Strait during austral summer. *Biogeochemistry* 168 (2), 1–19. <https://doi.org/10.1007/s10533-025-01226-7>.
- Droste, H., 2010. Sequence-stratigraphic framework of the Aptian Shu'aiba formation in the sultanate of Oman. In: van Buchem, F.S.P., Al-Husseini, M.I., Maurer, F., Droste, H.J. (Eds.), Barremian–Aptian Stratigraphy and Hydrocarbon Habitat of the Eastern Arabian Plate, Vol. I. *GeoArabia Special Publication 4*, pp. 229–283.
- Dunham, R.J., 1962. Classification of carbonate rocks according to depositional texture. In: Ham, W.E. (Ed.), *Classification of Carbonate Rocks*, American Association of Petroleum Geologists, Symposium, pp. 108–121.
- Embry, A.F., Klovan, J.E., 1971. A late Devonian reef tract on northeastern Banks Island, NWT. *Bull. Can. Petrol. Geol.* 19, 730–781. <https://doi.org/10.35767/gscpbull.19.4.730>.
- Erba, E., Tremolada, F., 2004. Nannofossil carbonate fluxes during the early Cretaceous: Phytoplankton response to nitrification episodes, atmospheric CO₂, and anoxia. *Paleoceanography* 19 (1). <https://doi.org/10.1029/2003PA000884>.
- Erba, E., James Claps, M., Jones, C., Larson, R., Opdyke, B., Silva I., Premoli, Riva, A., Salvini, G., Torricelli, S., 1999. Integrated stratigraphy of the Cismon Apticore (southern Alps, Italy); a reference section for the Barremian-Aptian interval at low latitudes. *J. Foraminif. Res.* 29 (4), 371–391.
- Erba, E., Bottini, C., Weissert, H.J., Keller, C.E., 2010. Calcareous nannoplankton response to surface-water acidification around Oceanic Anoxic Event 1a. *Science* 329 (5990), 428–432. <https://doi.org/10.1126/science.1188886>.
- Erba, E., Duncan, R.A., Bottini, C., Tiraboschi, D., Weissert, H., Jenkyns, H.C., Malinverno, A., 2015. Environmental consequences of Ontong Java Plateau and Kerguelan plateau volcanism. *Geol. Soc. Am. Spec. Pap.* 511, 271–303.
- Erba, E., Bottini, C., Faucher, G., Gambacorta, G., Visentin, S., 2019. The response of calcareous nannoplankton to Oceanic Anoxic events: the Italian pelagic record. *Boll. Soc. Paleontol. Ital.* 58 (1), 52.
- Erbacher, J., Thurow, J., Littke, R., 1996. Evolution patterns of radiolaria and organic matter variations: a new approach to identify sea-level changes in mid-Cretaceous pelagic environments. *Geology* 24 (6), 499–502. [https://doi.org/10.1130-0091-7613\(1996\)024%3C0499:eporao%3E2.3;2](https://doi.org/10.1130-0091-7613(1996)024%3C0499:eporao%3E2.3;2).
- Granier, B., 2014. Comment on "early Aptian paleoenvironmental evolution of the Bab Basin at the southern Neo-Tethys margin: response to global carbon-cycle perturbations across Ocean Anoxic Event 1a" by K. Yamamoto et al. *Geochim. Geophys. Geosyst.* 15 (5), 2086–2090. <https://doi.org/10.1002/2014GC005350>.
- Granier, B., Busnardo, R., 2013. New stratigraphic data on the Aptian of the Persian Gulf. *Cretac. Res.* 39, 170–182. <https://doi.org/10.1016/j.cretres.2012.02.011>.
- Haq, B.U., 2014. Cretaceous eustasy revisited. *Glob. planet. change* 113, 44–58. <https://doi.org/10.1016/j.gloplacha.2013.12.007>.
- Herdoca, C., Maurrasse, F.J., 2025. Geochemical response of aptian sediments before, during and after oceanic anoxic event 1a: insight from the la frontera section subbetic basin, southern Spain. *Front. Earth Sci.* 13, 1547237. <https://doi.org/10.3389/feart.2025.1547237>.
- Herrle, J.O., Köbler, P., Friedrich, O., Erlenkeuser, H., Hemleben, C., 2004. High-resolution carbon isotope records of the Aptian to lower Albian from SE France and the Mazagan Plateau (DSDP Site 545): a stratigraphic tool for paleoceanographic and paleobiologic reconstruction. *Earth Planet. Sci. Lett.* 218 (1–2), 149–161. [https://doi.org/10.1016/s0012-821x\(03\)00646-0](https://doi.org/10.1016/s0012-821x(03)00646-0).
- Hillgärtner, H., van Buchem, F., Gaumet, F., Razin, P., Pittet, B., Grötsch, J., Droste, H., 2003. The Barremian-Aptian evolution of the eastern Arabian carbonate platform margin (northern Oman). *J. Sediment. Res.* 73 (5), 756–773. <https://doi.org/10.1306/030503730756>.
- Hönisch, B., Ridgwell, A., Schmidt, D.N., Thomas, E., Gibbs, S.J., Sluijs, A., Zeebe, R., Kump, L., Martindale, R.C., Greene, S.E., et al., 2012. The geological record of ocean acidification. *Science* 335 (6070), 1058–1063. <https://doi.org/10.1126/science.1208277>.
- Hu, X., Zhao, K., Yilmaz, I.O., Li, Y., 2012. Stratigraphic transition and palaeoenvironmental changes from the Aptian oceanic anoxic event 1a (OAE1a) to the oceanic red bed 1 (ORB1) in the Yenicesihlar section, central Turkey. *Cretaceous Research* 38, 40–51.
- Huetter, A., Huck, S., Bodin, S., Heimhofer, U., Weyer, S., Klaus, P., Jochum, Immenhauser, A., 2019. Central Tethyan platform-top hypoxia during Oceanic Anoxic Event 1a. *Climate of the Past* 15 (4), 1327–1344. <https://doi.org/10.5194/cp-15-1327-2019>.
- Huck, S., Wohlwend, S., Coimbra, R., Christ, N., Weissert, H., 2017. Disentangling shallow-water bulk carbonate carbon isotope archives with evidence for multi-stage diagenesis: an in-depth component-specific petrographic and geochemical study from Oman (mid-Cretaceous). *Depositional Rec.* 3 (2), 233–257. <https://doi.org/10.1002/dep2.35>.
- Hughes, G.W., 2000. Bioestratigraphy of the Shu'aiba Formation, Shaybah field, Saudi Arabia. *GeoArabia* 5 (4), 545–578. <https://doi.org/10.2113/geoarabia0504545>.
- Immenhauser, A., 2021. On the delimitation of the carbonate burial realm. *Depositional Rec.* 8 (2), 524–574. <https://doi.org/10.1002/dep2.173>.
- Immenhauser, A., Kenter, J.A., Ganssen, G., Bahamonde, J.R., van Vliet, A., Saher, M.H., 2002. Origin and significance of isotope shifts in Pennsylvanian carbonates (Asturias, NW Spain). *J. Sediment. Res.* 72 (1), 82–94.

- Immenhauser, A., Della Porta, G., Kenter, J.A., Bahamonde, J.R., 2003. An alternative model for positive shifts in shallow-marine carbonate $\delta^{13}\text{C}$ and $\delta^{18}\text{O}$. *Sedimentology* 50 (5), 953–959. <https://doi.org/10.1046/j.1365-3091.2003.00590.x>.
- Immenhauser, A., Hillgärtner, H., van Bentum, E., 2005. Microbial-foraminiferal episodes in the early Aptian of the southern Tethyan margin: ecological significance and possible relation to oceanic anoxic event 1a. *Sedimentology* 52 (1), 77–99. <https://doi.org/10.1111/j.1365-3091.2004.00683.x>.
- Immenhauser, A., Schläger, W., Burns, S.J., Scott, R.W., Geel, T., Lehmann, J., van der Gaast, S., Bolder-Schrijver, 1999. Late Aptian to late Albian sea-level fluctuations constrained by geochemical and biological evidence (Nahr Umr Formation, Oman). *J. Sediment. Res.* 69 (2), 434–446. <https://doi.org/10.2110/jsr.69.434>.
- Jafarian, A., Husinec, A., Wang, C., Chen, X., Saboor, A., Li, Y., 2023. Aptian Oceanic Anoxic Event 1a in the shallow, carbonate-dominated intrashelf Kazhdumi Basin, Zagros Mountains. *Sedimentology* 70 (6), 1981–2014. <https://doi.org/10.1111/sed.13102>.
- Jafarian, A., Husinec, A., Wang, C., Chen, X., Wang, M., Gröcke, D.R., Saboor, A., Li, Y., 2024. Intrashelf basin record of redox and productivity changes along the Arabian margin of Neo-Tethys during Oceanic Anoxic Event 1a. *Palaeogeogr. Palaeoclimatol. Palaeoecol.* 636, 111975. <https://doi.org/10.1016/j.palaeo.2023.111975>.
- Jahn, A., Lindsay, K., Giraud, X., Gruber, N., Otto-Btiesner, B.L., Liu, Z., Brady, E.C., 2014. Carbon isotopes in the ocean model of the Community Earth System Model (CESM1). *Geosci. Model Dev. Discuss.* 7 (6), 7461–7503. <https://doi.org/10.5194/gmd-8-2419-2015>.
- Jenkyns, H.C., 2010. Geochemistry of oceanic anoxic events. *Geochem. Geophys. Geosyst.* 11 (3), 1–30. <https://doi.org/10.1029/2009gc002788>.
- Kocsis, A.T., Scotese, C.R., 2021. Mapping paleocoastlines and continental flooding during the Phanerozoic. *Earth Sci. Rev.* 213, 103463. <https://doi.org/10.1016/j.earscirev.2020.103463>.
- Konert, G., Afifi, A., Al-Hajri, S.A., Drosté, H.J., 2001. Paleozoic stratigraphy and hydrocarbon habitats of the Arabian Plate. *GeoArabia* 6 (3), 407–442. <https://doi.org/10.2113/geoarabia0603407>.
- Kuhnt, W., Holbourn, A., Moullade, M., 2011. Transient global cooling at the onset of early Aptian oceanic anoxic event (OAE) 1a. *Geology* 39 (4), 323–326. <https://doi.org/10.1130/g31554.1>.
- Larson, R.L., 1991. Geological consequences of superplumes. *Geology* 19 (10), 963–966. [https://doi.org/10.1130/0091-7613\(1991\)019<0963:GCOS>2.3.CO;2](https://doi.org/10.1130/0091-7613(1991)019<0963:GCOS>2.3.CO;2).
- Li, Y.-X., Bralower, T.J., Montañez, I.P., Osleger, D.A., Arthur, M.A., Bice, D.M., Herbert, T.D., Erba, E., Premoli Silva, I., 2008. Toward an orbital chronology for the early Aptian Oceanic Anoxic Event (OAE1a, ~120 Ma). *Earth Planet. Sci. Lett.* 271 (1), 88–100. <https://doi.org/10.1016/j.epsl.2008.03.055>.
- Lorenzen, J., Kuhnt, W., Holbourn, A., Flögel, S., Moullade, M., Tronchetti, G., 2013. A new sediment core from the Bedoulian (lower Aptian) stratotype at Roquefort-La Bédoule, SE France. *Cretac. Res.* 39, 6–16. <https://doi.org/10.1016/j.cretres.2012.03.019>.
- Malinverno, A., Erba, E., Herbert, T.D., 2010. Orbital tuning as an inverse problem: Chronology of the early Aptian oceanic anoxic event 1a (Selli Level) in the Cismón APTICORE. *Paleoceanography* 25 (2). <https://doi.org/10.1029/2009pa001769>.
- Martínez-Rodríguez, R., Batenburg, S.J., Castro, J.M., de Gea, G.A., Nieto, L.M., Ruiz-Ortiz, P.A., Robinson, S., 2024. Integrated cyclostratigraphy of the Cau core (SE Spain) - A timescale for climate change during the early Aptian Anoxic Event (OAE 1a) and the late Aptian. *Glob. Planet. Chang.* 104361–104361. <https://doi.org/10.1016/j.gloplacha.2024.104361>.
- Masse, J.-P., Chartrouse, A., Borgomanero, J., 1998. The lower Cretaceous (upper Barremian-lower Aptian) Caprinid rudists from Northern Oman. *Geobios* 31 (supplement 1), 211–223. [https://doi.org/10.1016/s0016-6995\(98\)80078-8](https://doi.org/10.1016/s0016-6995(98)80078-8).
- Maurer, F., Al-Mehsin, K., Pierson, B.J., Eberli, G.P., Warrlich, G., Drysdale, D., Drosté, H.J., 2010. Facies characteristics and architecture of upper Aptian Shu'aibah clinoforms in Abu Dhabi. In: van Buchem, F.S.P., Al-Husseini, M.I., Maurer, F., Drosté, H.J. (Eds.), Barremian–Aptian Stratigraphy and Hydrocarbon Habitat of the Eastern Arabian Plate, Vol. II. *GeoArabia Special Publication* 4, pp. 445–468.
- Menegatti, A.P., Weissert, H., Brown, R.S., Tyson, R.V., Farrimond, P., Strasser, A., Caron, M., 1998. High-resolution $\delta^{13}\text{C}$ stratigraphy through the early Aptian “Livello Selli” of the Alpine Tethys. *Paleoceanography* 13 (5), 530–545. <https://doi.org/10.1029/98pa01793>.
- Moosavizadeh, M.A., Mahboubi, A., Moussavi-Harami, R., Kavoosi, M.A., 2013. Early Aptian oceanic anoxic event (OAE 1a) in Northeastern Arabian Plate setting: an example from Dariyan Formation in Zagros fold-thrust belt, SE Iran. *Arab. J. Geosci.* 7 (11), 4745–4756. <https://doi.org/10.1007/s12517-013-1025-z>.
- Moosavizadeh, S.M.A., Mahboubi, A., Moussavi-Harami, R., Kavoosi, M.A., Schlagintweit, F., 2015. Sequence stratigraphy and platform to basin margin facies transition of the lower Cretaceous Dariyan Formation (northeastern Arabian Plate, Zagros fold-thrust belt, Iran). *Bull. Geosci.* 145–172. <https://doi.org/10.3140/bull.geosci.1413>.
- Moullade, M., Tronchetti, G., Granier, B., Bornemann, A., Kuhnt, W., Lorenzen, J., 2015. High-resolution integrated stratigraphy of the OAE1a and enclosing strata from core drillings in the Bedoulian stratotype (Roquefort-La Bédoule, SE France). *Cretac. Res.* 56, 119–140. <https://doi.org/10.1016/j.cretres.2015.03.004>.
- Mutterlose, J., Bottini, C., 2013. Early Cretaceous chalks from the North Sea giving evidence for global change. *Nat. Commun.* 4, 1686. <https://doi.org/10.1038/ncomms2698>.
- Naafs, B.D.A., Castro, J.M., de Gea, G.A., Quijano, M.L., Schmidt, D.N., Pancost, R.D., 2016. Gradual and sustained carbon dioxide release during Aptian Oceanic Anoxic Event 1a. *Nat. Geosci.* 9 (2), 135–139. <https://doi.org/10.1038/ngeo2627>.
- Naderi-Khujin, M., Seyrafian, A., Vaziri-Moghaddam, H., Tavakoli, V., 2016. A record of global change: OAE 1a in Dariyan shallow-water platform carbonates, southern Tethys, Persian Gulf, Iran. *Facies* 62 (4). <https://doi.org/10.1007/s10347-016-0476-6>.
- Núñez-Useche, F., Barragán, R., Moreno-Bedmar, J.A., Canet, C., 2015. Geochemical and paleoenvironmental record of the early to early late Aptian major episodes of accelerated change: evidence from Sierra del Rosario, Northeast Mexico. *Sediment. Geol.* 324, 47–66. <https://doi.org/10.1016/j.sedgeo.2015.04.006>.
- Percival, L.M.E., Tedeschi, L.R., Creaser, R.A., Bottini, C., Erba, E., Giraud, F., Svensen, H., Savian, J., Trindade, R., Coccioni, R., et al., 2021. Determining the style and provenance of magmatic activity during the early Aptian Oceanic Anoxic Event (OAE 1a). *Glob. Planet. Chang.* 200, 1–18. <https://doi.org/10.1016/j.gloplacha.2021.103461>.
- Pierson, B., Eberli, G.P., Al-Mehsin, K., Al-Mehlali, S., Warrlich, G., Drosté, H.J., Maurer, F., Whitworth, J., Drysdale, D., 2010. Barremian–Aptian Stratigraphy and Hydrocarbon Habitat of the Eastern Arabian Plate. In: van Buchem, F.S.P., Al-Husseini, M.I., Maurer, F., Drosté, H.J. (Eds.), *Seismic stratigraphy and depositional history of the Upper Shu'aibah (Late Aptian) in the UAE and Oman*, vol. II. *GeoArabia Special Publication* 4, pp. 411–444.
- Pittet, B., van Buchem, F.S.P., Hillgärtner, H., Razin, P., Groetsch, J., Drosté, H., 2002. Ecological succession, palaeoenvironmental change, and depositional sequences of Barremian–Aptian shallow-water carbonates in northern Oman. *Sedimentology* 49 (3), 555–581. <https://doi.org/10.1046/j.1365-3091.2002.00460.x>.
- Pohl, A., Donnadieu, Y., Godderis, Y., Lanteaume, C., Hairabedian, A., Frau, C., Michel, J., Laugie, M., Reijmer, J.J.G., Scotese, C.R., Borgomanero, J., 2020. Carbonate platform production during the Cretaceous. *Geol. Soc. Am. Bull.* 132, 2606–2610. <https://doi.org/10.1130/B35680.1>.
- Rameil, N., Immenhauser, A., Warrlich, G., Hillgartner, H., Drosté, H.J., 2010. Morphological patterns of Aptian Lithocodium–Bacinella geobodies: relation to environment and scale. *Sedimentology* 57 (3), 883–911. <https://doi.org/10.1111/j.1365-3091.2009.0124x>.
- Rameil, N., Immenhauser, A., Csoma, A.E., Warrlich, G., 2012. Surfaces with a long history: the Aptian top Shu'aibah Formation unconformity, Sultanate of Oman. *Sedimentology* 59 (1), 212–248. <https://doi.org/10.1111/j.1365-3091.2011.01279.x>.
- Sattler, U., Immenhauser, A., Hillgärtner, H., Esteban, M., 2005. Characterization, lateral variability and lateral extent of discontinuity surfaces on a Carbonate Platform (Barremian to lower Aptian, Oman). *Sedimentology* 52 (2), 339–361. <https://doi.org/10.1111/j.1365-3091.2005.00701.x>.
- Schlager, W., 2003. Benthic carbonate factories of the Phanerozoic. *Int. J. Earth Sci.* 92, 445–464.
- Schroeder, R., 1975. General evolutionary trends in Orbitolinines. *Rev. Esp. Micropaleontol. Numero Especial* 117–128.
- Schroeder, R., van Buchem, F.S.P., Cherchi, A., Baghbani, D., Vincent, B., Immenhauser, A., Granier, B., 2010. Revised orbitolinid biostratigraphic zonation for the Barremian–Aptian of the eastern Arabian Plate and implications for regional stratigraphic correlations. In: van Buchem, F.S.P., Al-Husseini, M.I., Maurer, F., Drosté, H.J. (Eds.), *Barremian–Aptian Stratigraphy and Hydrocarbon Habitat of the Eastern Arabian Plate*, vol. I. *GeoArabia Special Publication* 4, pp. 49–96.
- Scott, R.W., 2016. Barremian–Aptian–Albian carbon isotope segments as chronostratigraphic signals: numerical age calibration and durations. *Stratigraphy* 13 (1), 21–46. <https://doi.org/10.29041/strat.13.1.02>.
- Sharland, P.R., Archer, R., Casey, D., Davies, R.B., Hall, S., Heward, A.P., Horbury, A., Simmons, M., 2001. *Arabian Plate Sequence Stratigraphy*, vol. 2. *GeoArabia Special Publication*, pp. 1–371.
- Simmons, M.D., 1994. *Micropalaeontology and Hydrocarbon Exploration in the Middle East*.
- Simmons, M.D., Hart, M.B., 1987. The biostratigraphy and microfacies of the early to Mid-Cretaceous of Wadi Mi'aidin, Central Oman Mountains. In: Hart, M.B. (Ed.), *Micropalaeontology of Carbonate Environments*. Chichester, UK, Ellis Horwood, pp. 176–207.
- Simmons, M.D., Whittaker, J.A., Jones, R.W., 2000. Orbitolinids from Cretaceous sediments of the Middle East – a revision of the F.R.S. Henson and Associates Collection. In: Hart, M.B., Kaminski, M.A., Smart, C.W. (Eds.), *Proceedings of the Fifth International Workshop on Agglutinated Foraminifera*, vol. 7. Grzybowski Foundation special Publication, pp. 411–437.
- Simmons, M.D., Sharland, P.R., Casey, D.M., Davies, R.B., Sutcliffe, O.E., 2007. Arabian Plate sequence stratigraphy: potential implications for global chronostratigraphy. *GeoArabia* 12 (4), 101–130. <https://doi.org/10.2113/geoarabia120410>.
- Skelton, P.W., Gili, E., 2012. Rudists and carbonate platforms in the Aptian: a case study on biotic interactions with ocean chemistry and climate. *Sedimentology* 59 (1), 81–117. <https://doi.org/10.1111/j.1365-3091.2011.01292.x>.
- Steuber, T., Veizer, J., 2002. Phanerozoic record of plate tectonic control of seawater chemistry and carbonate sedimentation. *Geology* 30 (12), 1123–1126. [https://doi.org/10.1130/0091-7613\(2002\)030<1123:PROTC>2.0.CO;2](https://doi.org/10.1130/0091-7613(2002)030<1123:PROTC>2.0.CO;2).
- Steuber, T., Rauch, M., Masse, J.-P., Graaf, J., Malkoc, M., 2005. Low-latitude seasonality of Cretaceous temperatures in warm and cold episodes. *Nature* 437 (7063), 1341–1344. <https://doi.org/10.1038/nature04096>.
- Steuber, T., Alsuwaidi, M., Hennhoefer, D., Sulieman, H., AlBlooshi, A., McAlpin, T.D., Shebl, H., 2022. Environmental change and carbon-cycle dynamics during the onset of Cretaceous oceanic anoxic event 1a from a carbonate-ramp depositional system, Abu Dhabi, U.A.E. *Palaeogeogr. Palaeoclimatol. Palaeoecol.* 601, 1–11. <https://doi.org/10.1016/j.palaeo.2022.111086>.
- Steuber, T., Löser, H., Mutterlose, J., Parente, M., 2023. Biogeodynamics of Cretaceous marine carbonate production. *Earth Sci. Rev.* 238, 2–43. <https://doi.org/10.1016/j.earscirev.2023.104341>.

- Stoll, H.M., Schrag, D.P., 2001. Sr/Ca variations in Cretaceous carbonates: relation to productivity and sea level changes. *Palaeogeogr. Palaeoclimatol. Palaeoecol.* 168 (3–4), 311–336. [https://doi.org/10.1016/s0031-0182\(01\)00205-x](https://doi.org/10.1016/s0031-0182(01)00205-x).
- Strohmenger, C.J., Weber, L.J., Ghani, A., Al-Mehsin, K., Al-Jeelani, O., Al-Mansoori, A., Al-Dayyani, T., Vaughan, L., Khan, S.A., Mitchell, J.C., 2006. High-resolution sequence stratigraphy and reservoir characterization of Upper Thamama (Lower Cretaceous) reservoirs of a giant Abu Dhabi oil field, United Arab Emirates. In: Harris, P.M., Weber, L.J. (Eds.), *Giant Hydrocarbon Reservoirs of the World: From Rocks to Reservoir Characterization and Modeling*. American Association of Petroleum Geosciences Memoir 88/SEPM Special Publication, pp. 139–171. <https://doi.org/10.1306/1215876M883271>.
- Strohmenger, C.J., Steuber, T., Ghani, A., Barwick, D.G., Al-Mazrooei, S.H.A., Al-Zaabi, N.O., 2010. Sedimentology and chemostratigraphy of the Hawar and Shu'aiba depositional sequences, Abu Dhabi, United Arab Emirates. In: van Buchem, F.S.P., Al-Husseini, M.I., Maurer, F., Droste, H.J. (Eds.), *Barremian–Aptian Stratigraphy and Hydrocarbon Habitat of the Eastern Arabian Plate*, vol. II. *GeoArabia Special Publication* 4, pp. 341–365.
- Swart, P.K., Eberli, G., 2005. The nature of the $\delta^{13}\text{C}$ of periplatform sediments: Implications for stratigraphy and the global carbon cycle. *Sediment. Geol.* 175 (1–4), 115–129. <https://doi.org/10.1016/j.sedgeo.2004.12.029>.
- Tejada, M.L.G., Suzuki, K., Kuroda, J., Coccioni, R., Mahoney, J.J., Ohkouchi, N., Sakamoto, T., Tatsumi, Y., 2009. Ontong Java Plateau eruption as a trigger for the early Aptian oceanic anoxic event. *Geology* 37 (9), 855–858. <https://doi.org/10.1130/g25763a.1>.
- Vahrenkamp, V.C., 1996. Carbon-isotope stratigraphy of the Upper Kharai and Shuaiba Formations: implications for the early Cretaceous evolution of the Arabian Gulf region. *Am. Assoc. Pet. Geol. Bull.* 80 (5), 647–662. <https://doi.org/10.1306/64ED8868-1724-11D7-8645000102C1865D>.
- Vahrenkamp, V.C., 2010. Chemostratigraphy of the Lower Cretaceous Shu'aiba Formation: A $\delta^{13}\text{C}$ reference profile for the Aptian Stage from the southern Neo-Tethys Ocean. In: van Buchem, F.S.P., Al-Husseini, M.I., Maurer, F., Droste, H.J. (Eds.), *Barremian–Aptian Stratigraphy and Hydrocarbon Habitat of the Eastern Arabian Plate*, vol. I. *GeoArabia Special Publication* 4, pp. 107–137.
- van Buchem, F.S.P., Pittet, B., Hillgärtner, H., Grötsch, J., Al Mansouri, A., Billing, I., Droste, H., Oterdoom, W., van Steenwinkel, M., 2002. High-resolution Sequence Stratigraphic Architecture of Barremian/Aptian Carbonate Systems in Northern Oman and the United Arab Emirates (Kharai and Shu'aiba Formations). *GeoArabia* 7 (3), 451–500.
- van Buchem, F.S.P., Al-Husseini, M.I., Maurer, F., Droste, F., Yose, L.A., 2010a. Sequence-stratigraphic synthesis of the Barremian–Aptian of the eastern Arabian Plate and implications for the petroleum habitat. In: van Buchem, F.S.P., Al-Husseini, M.I., Maurer, F., Droste, H.J. (Eds.), *Barremian–Aptian Stratigraphy and Hydrocarbon Habitat of the Eastern Arabian Plate*, vol. I. *GeoArabia Special Publication* 4, pp. 9–48.
- van Buchem, F.S.P., Baghbani, D., Bulot, L.G., Caron, M., Gaumet, F., Hosseini, A., Keyvani, F., Schroeder, R., Swennen, R., Vedrenn, V., Vincent, B., 2010b. Barremian–lower Albian sequence stratigraphy of southwest Iran (Gadwan, Dariyan and Kazhdumi formations) and its comparison with Oman, Qatar and United Arab Emirates. In: van Buchem, F.S.P., Al-Husseini, M.I., Maurer, F., Droste, H.J. (Eds.), *Barremian–Aptian Stratigraphy and Hydrocarbon Habitat of the Eastern Arabian Plate*, vol. I. *GeoArabia Special Publication* 4, pp. 503–548.
- Vincent, B., van Buchem, F.S.P., Bulot, L.G., Immenhauser, A., Caron, M., Baghbani, D., Huc, A.Y., 2010. Carbon-isotope stratigraphy, biostratigraphy and organic matter distribution in the Aptian – lower Albian successions of southwest Iran (Dariyan and Kazhdumi formations). In: van Buchem, F.S.P., Al-Husseini, M.I., Maurer, F., Droste, H.J. (Eds.), *Barremian–Aptian Stratigraphy and Hydrocarbon Habitat of the Eastern Arabian Plate*, vol. I. *GeoArabia Special Publication* 4, pp. 139–166.
- Weissert, H., Erba, E., 2004. Volcanism, CO_2 and palaeoclimate: a late Jurassic–early Cretaceous carbon and oxygen isotope record. *J. Geol. Soc. Lond.* 161 (4), 659–702. <https://doi.org/10.1144/0016-764903-087>.
- Weissert, H., Lini, A., Föllmi, K.B., Kuhn, O., 1998. Correlation of early Cretaceous carbon isotope stratigraphy and platform drowning events: a possible link? *Palaeogeogr. Palaeoclimatol. Palaeoecol.* 137 (3–4), 189–203. [https://doi.org/10.1016/S0031-0182\(97\)00109-0](https://doi.org/10.1016/S0031-0182(97)00109-0).
- Wissler, L., Funk, H., Weissert, H., 2003. Response of early Cretaceous carbonate platforms to changes in atmospheric carbon dioxide levels. *Palaeogeogr.* *Palaeoclimatol.* *Palaeoecol.* 200 (1–4), 187–205. [https://doi.org/10.1016/s0031-0182\(03\)00450-4](https://doi.org/10.1016/s0031-0182(03)00450-4).
- Witt, W., Gökdag, H., 1994. Orbitolinid biostratigraphy of the Shu'aiba Formation (Aptian), Oman—implications for reservoir development. *Micropalaeontology and hydrocarbon exploration in the Middle East*, 440, 221–241.
- Yamamoto, K., Ishibashi, M., Takayanagi, H., Asahara, Y., Sato, T., Nishi, H., Iryu, Y., 2013. Early Aptian paleoenvironmental evolution of the Bab Basin at the southern Neo-Tethys margin: response to global carbon-cycle perturbations across Ocean Anoxic Event 1a. *Geochem. Geophys. Geosyst.* 14 (4), 1104–1130. <https://doi.org/10.1002/ggge.20083>.
- Yang, C.S., Kao, S.P., Lee, F.B., Hung, P.S., 2004. Twelve different interpolation methods: A case study of Surfer 8.0. In: *Proceedings of the XXth ISPRS Congress*, Vol. 35, pp. 778–785.
- Yose, L.A., Ruf, A.S., Strohmenger, C.J., Al-Hosani, I., Al-Maskary, S., Bloch, G., Al-Mehairi, Y., Schuelke, J.S., Gombos, A., Johnson, I.G., 2006. In: Harris, P.M., Weber, L.J. (Eds.), *Hydrocarbon Reservoirs of the World: From Rocks to Reservoir Characterization and Modeling*, 88. American Association of Petroleum Geologists, Memoir, pp. 173–212. <https://doi.org/10.1306/1215877M882562>.
- Yose, L.A., Strohmenger, C.J., Al-Hosani, I., Bloch, G., Al-Mehairi, Y., 2010. Sequence-stratigraphic evolution of an Aptian carbonate platform (Shu'aiba Formation), eastern Arabian Plate, onshore Abu Dhabi, United Arab Emirates. In: van Buchem, F.S.P., Al-Husseini, M.I., Maurer, F., Droste, H.J. (Eds.), *Barremian–Aptian Stratigraphy and Hydrocarbon Habitat of the Eastern Arabian Plate*, vol. II. *GeoArabia Special Publication* 4, pp. 309–340.
- Zhang, S., Zhou, R., DePaolo, D.J., 2019. The seawater Sr/Ca ratio in the past 50 Myr from bulk carbonate sediments corrected for diagenesis. *Earth Planet. Sci. Lett.* 530, 115949. <https://doi.org/10.1016/j.epsl.2019.115949>.